Petroleum Science 23 (2026) 2390–2403

Contents lists available at ScienceDirect

Petroleum Science

journal homepage: www.keaipublishing.com/en/journals/petroleum-science

Original Paper

Source and thermochemical sulfate reduction of natural gases in the Ordovician carbonate–evaporite assemblage in the Ordos Basin, China

Xiao-Yan Chen [a,*], Wen-Hui Liu [a], Hou-Yong Luo [b,**], Xiao-Feng Wang [a], Liu-Bin Wei [c], Dong-Dong Zhang [a], Wen Zhang [a], Wen-Qing Wang [d]

[a] State Key Laboratory of Continental Evolution and Early Life, Department of Geology, Northwest University, Xi'an, 710069, Shaanxi, China
[b] College of Chemistry and Chemical Engineering, Shaanxi University of Science & Technology, Xi'an, 710021, Shaanxi, China
[c] Research Institute of Exploration and Development, PetroChina Changqing Oilfield, Xi'an, 710018, Shaanxi, China
[d] School of Earth Sciences and Engineering, Xi'an Shiyou University, Xi'an, 710065, Shaanxi, China

ARTICLE INFO

Article history:
Received 6 January 2025
Received in revised form
11 December 2025
Accepted 2 March 2026
Available online 7 March 2026

Edited by Xiu-Fang Hu

Keywords:
Carbonate–evaporite assemblage
Thermochemical sulfate reduction
Gas source identification
Subsalt gas accumulation
Ordovician
Ordos Basin

ABSTRACT

Thermochemical sulfate reduction (TSR) commonly occurs in carbonate–evaporite assemblages, making the identification of gas sources difficult. Given that the sources of natural gases in the Ordovician carbonate–evaporite assemblage of the Ordos Basin remain unclear, this study was conducted to reveal gas sources and TSR characteristics by geochemical and mineralogical analyses. The results showed that the C_1/C_{1-5} and $\delta^{13}C_2$ values of the Ordovician subsalt gases were higher than those only affected by thermal evolution owing to the selective consumption of the C_{2-5} components by TSR reaction. For some oil-type gases from the subsalt reservoirs, TSR even led to their $\delta^{13}C_2$ values reflecting to the characteristic of coal-type gas. TSR-mediated reformation of methane in the Ordovician subsalt gases was extremely weak, and $\delta^{13}C_1$ and δD_1 values confirmed that it originated primarily from marine source rocks. Cracks and caves of the Ordovician subsalt reservoirs were generally filled with TSR-related secondary calcite, elemental sulfur, and pyrite, but little bitumen coexisted, indicating that the major reductants of TSR reaction were gaseous hydrocarbons, particularly the C_{2-5} components. Expulsion of liquid hydrocarbons from the Majiagou source rocks to form paleo-oil reservoirs was severely limited because the source layer had a low total organic carbon content and contained gypsum–salt rocks. Thus, the Ordovician subsalt gas reservoirs had primarily formed through the direct migration and accumulation of gaseous hydrocarbons. Consequently, the primary gas reservoirs are the main targets for future natural gas exploration in the Ordovician carbonate–evaporite assemblage of the Ordos Basin.
© 2026 The Authors. Publishing services by Elsevier B.V. on behalf of KeAi Communications Co. Ltd. This is an open access article under the CC BY license (http://creativecommons.org/licenses/by/4.0/).

1. Introduction

Marine carbonate rocks are important reservoirs for oil and natural gas, yielding approximately 60% of global extraction and production. Among the carbonate oil and gas reservoirs discovered globally, approximately 46% reserves come from carbonate–evaporite assemblages (Hu et al., 2022). These oil- and gas-rich carbonate reservoirs are primarily distributed in the Late Paleozoic–Cenozoic layers, particularly in the Jurassic and Cretaceous strata of the Mesozoic era (Zhang et al., 2014). However, the proven carbonate reservoirs in China are primarily distributed in the Sinian–Paleozoic strata. Extensive research studies have shown that organic–inorganic interactions, particularly thermochemical sulfate reduction (TSR), occur easily in carbonate reservoirs, resulting in modifications in both petroleum geochemistry and reservoir quality (Cai et al., 2001, 2003, 2004, 2005, 2009, 2014, 2016, 2022; Dai, 1985; Guo et al., 2022a, 2022b; Hao et al., 2008; Jiang et al., 2018; Liu et al., 2018; Seewald, 2003; Toland, 1960; Zhu et al., 2014). TSR involves the reaction of hydrocarbons with sulfate ions dissolved in formation water, which generates by-products such as CO_2 and H_2S. Consequently, the hydrocarbon composition is modified, and the stable isotopic signatures of both residual hydrocarbons and newly formed compounds also induce systematic shifts (Cai et al., 2022; Hao et al., 2008; Kiyosu and Krouse, 1989; Liu et al., 2006, 2013,

* Corresponding author.
** Corresponding author.
E-mail addresses: chenxy@nwu.edu.cn (X.-Y. Chen), luohouyong@sust.edu.cn (H.-Y. Luo).
Peer review under the responsibility of China University of Petroleum (Beijing).

https://doi.org/10.1016/j.petsci.2026.03.004
1995-8226/© 2026 The Authors. Publishing services by Elsevier B.V. on behalf of KeAi Communications Co. Ltd. This is an open access article under the CC BY license (http://creativecommons.org/licenses/by/4.0/).

2014b, 2019, 2020; Machel, 1998; Worden et al., 1995; Zhang et al., 2007, 2008). Globally, nearly all high-H_2S-containing hydrocarbon reservoirs in carbonate formations are inherently associated with TSR, and these are predominantly found in carbonate–evaporite depositional systems (Anisimov, 1978; Dou et al., 2024; Fei et al., 2010; Heydari, 1997; Krouse et al., 1988; Orr, 1977). As a result, TSR creates challenges for identifying natural gas sources and analysing gas reservoir evolution based on geochemical indicators.

In recent years, the source and accumulation of natural gases in the Ordovician carbonate–evaporite assemblage of the Ordos Basin in China have been controversial topics (He et al., 2022; Kong et al., 2019, 2024; Wu et al., 2017; Yang et al., 2022; Zhang et al., 2023; Zhou et al., 2023). One viewpoint, based on the heavy carbon isotope composition of ethane, is that the subsalt gas reservoirs formed through mixing of the Upper Paleozoic coal-type and Lower Paleozoic oil-type gases (He et al., 2022; Wu et al., 2017). The other viewpoint, which is based on the carbon and hydrogen isotopes of methane, is that the subsalt gases are mainly derived from the Lower Paleozoic oil-type gas, and the heavy carbon isotope composition of ethane in the subsalt gases at low thermal maturity (equivalent vitrinite reflectance (R_o) < 1.5%) is mainly caused by TSR reformation (Kong et al., 2024; Yang et al., 2022; Zhang et al., 2023). It increasingly affects ethane carbon isotope values with thermal maturity increasing when equivalent R_o is more than 1.5% (Yang et al., 2022). Additionally, according to Yang et al. (2022), further studies are needed to understand the wide H_2S content range (1.27%–23.58%) in the subsalt gases and to determine why some low-maturity, H_2S-free gas samples display high ethane carbon isotope compositions.

This study aimed to elucidate the characteristics and influences of TSR for natural gases in the Ordovician carbonate–evaporite assemblage of the Ordos Basin and to reveal the source and evolution of the subsalt gas reservoirs by analysing gas compositions and isotope characteristics, secondary minerals in reservoir, and gas reservoir formation and reformation. Our results will provide valuable reference material to guide future research on gas sources and accumulation, as well as gas exploration in the marine carbonate–evaporite assemblage of the Ordos Basin.

2. Geological setting

The Ordos Basin, covering an area of 370,000 km^2 in north-central China, represents one of the regions in the country with the largest amounts of hydrocarbons (Yang and Pei, 1996). This structurally complex basin comprises six primary tectonic units (Fig. 1(a)): the Jinxi Fault-fold Belt in the east, which progressively transitions westward through the Yishan Slope and Tianhuan Depression to the Western Thrust Belt, complemented by the Yimeng Uplift to the north and Weibei Uplift to the south. The Yishan Slope, a monocline structure characterised by gentle westward dipping, serves as the principal area for Paleozoic gas accumulation, particularly its central and northern regions (Fig. 1(a)). The proven Paleozoic gas reservoirs in the Ordos Basin are primarily distributed in the Upper Paleozoic sedimentary strata, including the upper (P_2sh) and lower (P_2x) Shihezi, Shanxi (P_1s), Taiyuan (P_1t), and Benxi (C_2b) Formations, and the Lower Paleozoic Majiagou (O_1m) Formation, with gas originating mainly from the Upper Paleozoic coal-measure source rocks or Lower Paleozoic marine carbonate source rocks (Cai et al., 2005; Dai et al., 2005, 2014; He et al., 2022; Kong et al., 2024; Li et al., 2014, 2018; Liu et al., 2016; Zhang et al., 2023; Zhou et al., 2023).

As part of the North China Craton in the Paleozoic era (Huang et al., 2025a, 2025b), the Ordos Basin was primarily deposited as carbonate platforms during the Early Paleozoic period. In the Ordovician period, this basin developed extensive gypsum–halite depositional systems within its central-eastern sectors (Zhou et al., 2020), forming a characteristic carbonate–evaporite sedimentary assemblage within the Majiagou Formation (Fig. 1). The preserved Majiagou Formation in the Ordos Basin is divided into five distinct members according to the sedimentary cycles (Fig. 1(b)): two transgressive sequences (second and fourth members) of carbonate rocks, and three regressive sequences (first, third, and fifth members) of carbonate–evaporite rocks (Zhou et al., 2023). The source rocks of the Majiagou Formation developed primarily in the regressive sequence, particularly within the third (O_1m^3) and fifth (O_1m^5) members. The source rocks are mainly composed of type I kerogen because their organic matter was derived from algal-dominated aquatic organisms (Kong et al., 2024; Zhou et al., 2023). The current R_o value of the Ordovician top surface ranges from approximately 1.2% to 3.2%, and the R_o distribution characteristically exhibits high values in the south and low values in the north (Ren et al., 2021; Fig. 1(a)), which indicate that the Majiagou source rocks have reached high to over-maturity stages with a southward increase in maturity.

Studies have shown that the Ordovician Majiagou Formation in the Ordos Basin comprises two gas accumulation combinations: the post-salt and subsalt natural gas reservoirs (Fig. 1(b)). For the source of the post-salt gas reservoirs, one widely accepted understanding is that the natural gas is mainly coal-type gas from the Upper Paleozoic with some mixing of the Lower Paleozoic oil-type gas (Li et al., 2018; Liu et al., 2016; Zhang et al., 2023). As for the source of the subsalt gas reservoirs, different scholars support two distinct perspectives that are based on gas composition and isotope composition analyses. One perspective asserts that the source is a mix of both Upper Paleozoic coal-type and Lower Paleozoic oil-type gases, whereas the other perspective points to the Lower Paleozoic oil-type gas as being the only source (He et al., 2022; Kong et al., 2024; Zhang et al., 2023; Zhou et al., 2023).

3. Samples and methods

3.1. Natural gas components and stable isotope compositions

Fifteen gas sample s were collected from the subsalt gas reservoirs of the Majiagou Formation, and one gas sample was collected from the Upper Paleozoic gas reservoir. Natural gas components were analysed using an Agilent 7890B gas chromatograph (GC) equipped with a flame ionisation detector. The GC oven was set to 80 °C for 2 min, then heated to 100 °C at 5 °C/min, and finally to 290 °C at 10 °C/min with a 3 min hold. Carbon and hydrogen isotope compositions of all sixteen samples were analysed using a MAT253 Plus mass spectrometer and Trace1300 GC. The oven temperature of the GC was initially set at 80 °C for a 3 min hold and the increased to 190 °C at 15 °C/min with a final 5 min hold. Combustion furnace temperature was maintained at 960 °C for carbon isotope analysis, and cracking furnace temperature was held at 1350 °C for hydrogen isotope analysis. The $\delta^{13}C$ value was reported relative to the Vienna Pee Dee Belemnite standard and the δD value relative to the Vienna Standard Mean Ocean Water, with a measurement precision of ±0.3‰ and ±5‰, respectively. Natural gas analysis data are shown in Table 1.

3.2. Sulfur isotope composition

Eleven sulfur and six anhydrite samples from the subsalt reservoir of the Majiagou Formation were collected for sulfur isotope composition analysis. After powdered, a sample containing 60 μg of sulfur was transferred into the combustion tube of a Flash 2000HT element using its automatic sampler. The SO_2

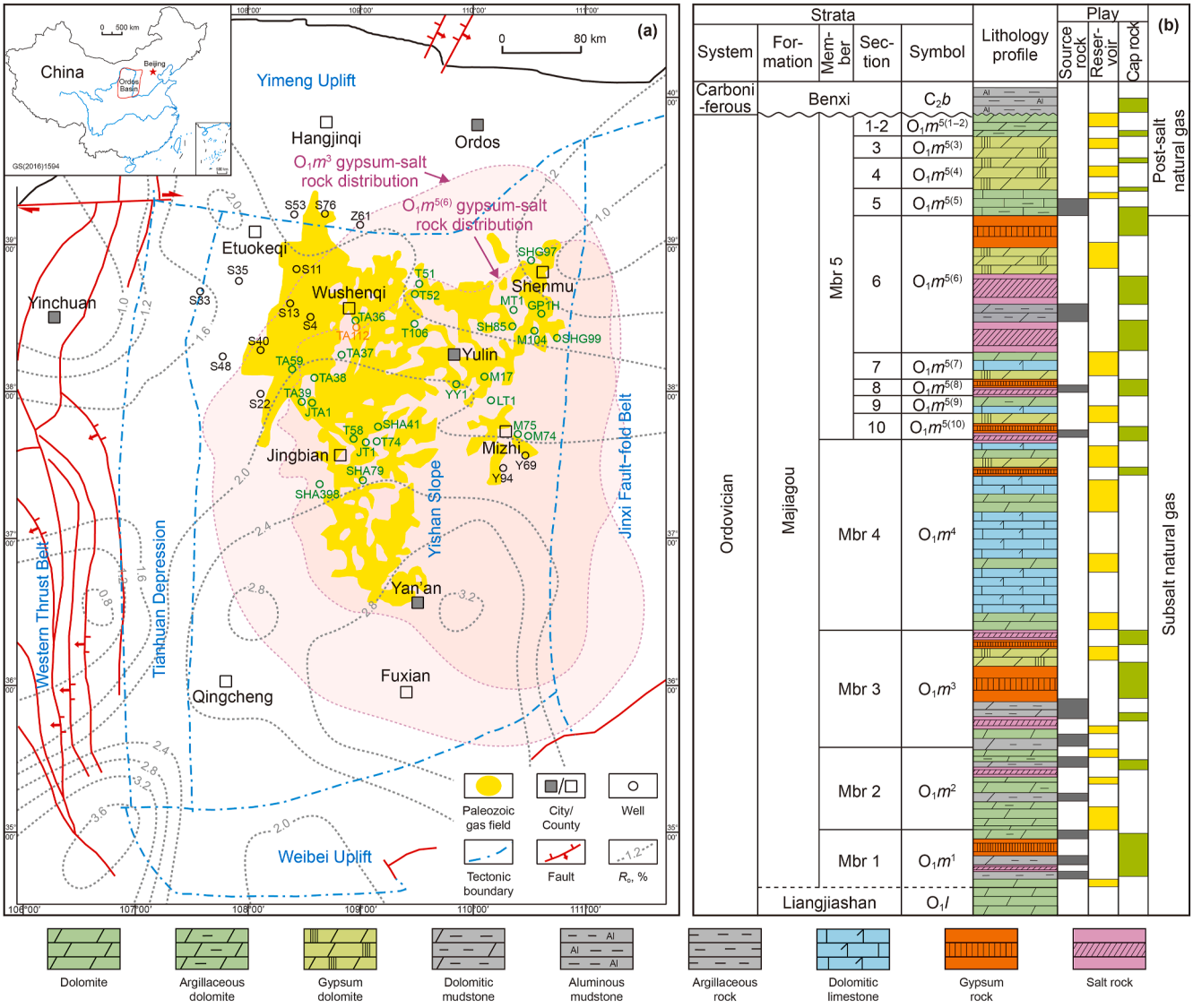

Fig. 1. **(a)** Geological tectonics in the Ordos Basin, distribution of the Paleozoic gasfields, the current R_o on the Ordovician top surface, and the locations of major sample wells (subsalt gas wells shown in green, and other representative Paleozoic gas wells shown in black); **(b)** stratigraphic profile of the Ordovician Majiagou Formation in the Ordos Basin (modified after Niu et al., 2024; Ren et al., 2021; Zhang et al., 2023). Mbr, Member.

generated in the combustion tube at 1020 °C was separated using a chromatographic column, and its sulfur isotope composition was analysed using a MAT253 Plus mass spectrometer. All $\delta^{34}S$ data (Table 2) are reported relative to the Vienna Canyon Diablo Troilite scale.

3.3. Microscopic observation of the rock sample

One rock sample from the O_1m^4 stratum (fourth member of the Majiagou Formation) of well JT1 was collected for argon ion beam polishing and scanning electron microscopy (SEM) observation. First, the sample was cut longitudinally and transversely. After rough polishing, the two cut surfaces were treated with six rounds of argon ion beam polishing for 2 h at accelerated voltages of 6.0, 5.5, 5.0, and 2.0 kV using a Leica EM TIC 3X thriple ion beam milling instrument under vacuum conditions. Subsequently, the polished surfaces were sprayed with a 2 nm gold film and finally observed at 10–20 kV using a Helios G4 UC electron microscope from Thermo Fisher Scientific.

4. Results and discussion

4.1. Composition and isotope characteristics of natural gases

Geochemical analysis results confirmed that the Upper Paleozoic natural gas in the Ordos Basin is coal-type gas derived from the Carboniferous–Permian coal-bearing strata (Cai et al., 2005; Dai et al., 2014; Li et al., 2014; Liu et al., 2007, 2009, 2019; Yu et al., 2013). The gas was characterised by high hydrocarbon gas content (average: >95%), enriched carbon isotope values of ethane ($\delta^{13}C_2$, higher than −28.0‰), with low hydrogen isotope values of methane (δD_1, mainly lower than −180‰). In contrast, natural gas from the subsalt reservoir of the Majiagou Formation exhibited significant differences in components and stable isotope compositions (Fig. 2).

Hydrocarbon gases from the subsalt reservoirs were primarily composed of methane (C_1), with a low content of wet gas components (C_{2-5}) (Table 1). Four subsalt gas samples from the E1, SHG97, and SHG99 wells showed the lowest C_1/C_{1-5} values

Table 1
Geochemical data of natural gases from the subsalt reservoirs of the Majiagou Formation and the Upper Paleozoic reservoirs in the Ordos Basin.

Number	Well	Reservoir	Composition, %						$\delta^{13}C$, ‰			δD_1, ‰	C_1/C_{1-5}	$\ln(C_1/C_2)$	$\ln(C_2/C_3)$	Data sources
			CH_4	C_2H_6	C_3H_8	CO_2	N_2	H_2S	CH_4	C_2H_6	C_3H_8					
Subsalt gas																
1	T52	O_1m^4	48.89	1.39	0.54	33.79	14.57	-	−42.1	−26.2	-	−167	0.949	3.560	0.945	This study
2	T51	O_1m^4	87.57	2.36	0.61	8.87	-	-	−41.7	−25.8	−24.6	−158	0.962	3.614	1.353	This study
3	M104	O_1m^4	45.36	1.00	0.24	0.32	52.05	-	−42.3	−25.4	-	−170	0.969	3.813	1.429	This study
4	GP1H	O_1m^4	80.62	0.48	0.18	11.38	6.61	-	−44.3	−27.6	−25.0	−188	0.991	5.124	0.981	This study
5	MT6	O_1m^4	92.00	3.46	1.15	0.27	1.51	-	−39.1	−24.7	-	-	0.938	3.281	1.102	This study
6	M172	O_1m^4	94.52	0.14	0.04	0.25	4.15	-	−37.9	-	-	-	0.998	6.515	1.253	This study
7	SH85	O_1m^4	92.44	0.29	0.19	1.79	4.98	-	−41.7	−20.8	−15.0	−151	0.992	5.764	0.423	This study
8	JT1	O_1m^4	74.35	1.31	0.19	-	21.91	-	−36.4	-	-	−144	0.979	4.039	1.931	This study
9	T106	O_1m^4	82.75	0.04	-	-	16.74	-	−37.2	-	-	−147	1.000	7.635	-	This study
10	TA59	O_1m^4	40.24	0.10	0.04	2.95	56.59	-	−38.5	-	-	-	0.996	5.997	0.916	This study
11	TA122	O_1m^4	28.17	0.01	-	4.74	67.01	-	−37.8	−19.1	-	−166	1.000	7.943	-	This study
12	YY1	O_1m^4	75.18	0.30	0.11	0.61	9.61	13.37	−40.4	−21.5	−17.9	−165	0.992	5.522	1.025	This study
13	TA90	O_1m^3	91.88	1.87	0.32	2.44	2.92	-	−40.7	−29.4	−24.6	−153	0.974	3.897	1.749	This study
14	J30	$O_1m^{5(7)}$	72.73	2.75	1.42	2.15	4.38	15.24	−33.9	−30.8	-	-	0.932	3.276	0.658	This study
15	J39	$O_1m^{5(6)}$	44.67	0.41	0.21	1.54	44.46	4.68	−36.5	−34.7	-	-	0.982	4.688	0.678	This study
16	SHA79	$O_1m^{5(5)}$	96.55	0.08	-	0.45	2.79	-	−37.3	−31.8	-	-	0.999	7.096	-	Dai et al., 2005
17	SHA41	$O_1m^{5(6-7)}$	98.14	1.51	0.20	-	-	-	−38.9	−28.7	−22.6	-	0.983	4.174	2.022	Liu et al., 2009
18	SHA398	$O_1m^{5(5)}$	99.11	0.25	0.12	-	-	-	−36.3	-	-	-	0.996	5.995	0.705	Yang and Liu, 2014
19	M17	O_1m^5	96.37	1.88	0.25	0.07	0.67	-	−35.1	−30.3	−26.5	-	0.971	3.935	2.027	Yang et al., 2009
20	E1	O_1m^2	80.38	11.62	4.12	-	-	-	−40.1	−32.7	-	-	0.804	1.934	1.037	Cai et al., 2005
21	TA51	O_1m^4	91.04	4.75	2.04	0.21	1.95	-	−42.1	−26.2	-	-	0.931	2.953	0.845	Kong et al., 2019
22	T58	$O_1m^{5(7)}$	82.96	0.05	0.03	2.41	1.85	12.76	−33.3	-	-	-	0.999	7.356	0.712	Kong et al., 2024
23	TA37	$O_1m^{5(10)}$	88.05	0.08	0.01	6.17	5.67	-	−38.2	−30.7	−20.0	-	0.999	6.979	2.104	Kong et al., 2024
24	M74	$O_1m^{5(5)}$	93.82	2.23	0.52	0.72	2.26	-	−40.0	−22.4	−20.7	-	0.967	3.738	1.452	Kong et al., 2024
25	M75	$O_1m^{5(5)}$	93.10	3.17	0.95	0.70	1.24	-	−40.2	−23.8	−23.1	-	0.949	3.381	1.206	Kong et al., 2024
26	LT1	$O_1m^{5(7)}$	96.87	1.79	0.28	0.07	0.67	-	−39.3	−23.8	−19.7	-	0.976	3.989	1.857	Kong et al., 2024
27	SHG99	$O_1m^{5(5)}$	81.17	7.94	3.85	1.17	3.32	-	−43.5	−31.4	−28.9	-	0.850	2.325	0.724	Kong et al., 2024
28	SHG97	$O_1m^{5(6-7)}$	70.85	7.31	3.30	9.77	6.85	-	−45.9	−31.1	−28.5	-	0.850	2.271	0.795	Kong et al., 2024
29	MT1	O_1m^4	90.82	3.38	0.99	1.34	2.33	3.30	−44.8	−27.7	−25.1	−169	0.943	3.290	1.229	Kong et al., 2024
30	TA36	O_1m^3	82.24	0.04	0.00	11.49	6.22	-	−37.3	−33.0	−25.8	−167	0.999	7.706	2.225	Kong et al., 2024
31	T74	$O_1m^{5(7)}$	88.64	0.76	0.12	0.83	8.42	1.27	−39.5	−29.9	−21.7	−174	0.989	4.754	1.868	Kong et al., 2024
32	T75	$O_1m^{5(6-7)}$	85.04	1.59	0.30	1.62	2.30	9.02	−32.4	−22.6	−22.4	-	0.977	3.981	1.666	Kong et al., 2024
33	T52	$O_1m^{5(10)}$	92.12	4.81	1.64	0.15	1.27	-	−41.7	−25.8	−24.6	-	0.935	2.952	1.074	Kong et al., 2024
34	JTA1	$O_1m^{5(7-9)}$	72.06	-	-	2.21	2.15	23.58	−36.0	−23.1	-	-	1.000	-	-	Liu et al., 2016
35	TA38	$O_1m^{5(7-9)}$	87.45	0.02	-	0.45	1.44	10.01	−35.8	−26.5	-	-	1.000	8.383	-	Liu et al., 2016
36	TA39	$O_1m^{5(6)}$	47.17	0.09	0.02	33.72	18.99	-	−38.1	−31.1	−21.9	-	0.997	6.262	1.504	Liu et al., 2016
37	TA39	$O_1m^{5(8)}$	32.30	0.02	0.01	31.68	35.98	-	−35.7	-	-	-	0.999	7.387	0.693	Liu et al., 2016
38	TA45	$O_1m^{5(6)}$	73.87	0.34	0.31	3.66	21.37	-	−39.1	−35.6	−26.6	-	0.985	5.381	0.092	Liu et al., 2016
39	SHG97	$O_1m^{5(4-5)}$	65.77	6.74	3.30	12.23	10.06	-	−45.8	−31.9	−29.5	-	0.846	2.278	0.714	Liu et al., 2016
Upper Paleozoic gas																
40	Y94	P_1s	87.77	2.01	0.12	0.01	9.98	-	−32.7	−20.8	−24.4	−177	0.976	3.776	2.818	This study
41	SD28-45	P_2x	93.39	3.55	0.57	-	-	-	−32.5	−24.1	−24.0	−193	0.955	3.270	1.829	Li et al., 2014
42	SD33-38	P_2x	94.82	2.85	0.39	-	-	-	−31.4	−23.1	−23.4	−192	0.965	3.505	1.989	Li et al., 2014
43	SD37-44	P_2x	94.18	3.36	0.54	-	-	-	−33.3	−24.3	−23.7	−182	0.958	3.333	1.828	Li et al., 2014
44	S6-01-15	P_2x	91.95	3.92	0.88	-	-	-	−32.3	−23.7	−24.5	−194	0.945	3.155	1.494	Li et al., 2014
45	S6-10-19	P_2x	92.50	3.76	0.78	-	-	-	−33.2	−24.4	−24.6	−194	0.949	3.203	1.573	Li et al., 2014
46	S14-22-41	P_1s	91.74	4.81	1.25	-	-	-	−32.6	−23.6	−23.4	−193	0.932	2.948	1.348	Li et al., 2014
47	S36-17-20	P_1s	93.27	3.91	0.74	-	-	-	−33.2	−24.4	−24.3	−194	0.949	3.172	1.665	Li et al., 2014
48	S36-10-9	P_1s	92.45	3.52	0.73	-	-	-	−34.0	−25.1	−25.7	−193	0.953	3.268	1.573	Li et al., 2014
49	S4-J1	P_1s	92.46	4.68	1.22	-	-	-	−32.9	−23.6	−22.9	−190	0.933	2.983	1.344	Li et al., 2014
50	SD23-54	P_1s	94.33	2.67	0.34	-	-	-	−32.7	−23.6	−24.2	−185	0.968	3.565	2.061	Li et al., 2014
51	SD37-62	P_1s	95.29	3.34	0.40	-	-	-	−32.5	−23.7	−23.6	−186	0.960	3.351	2.122	Li et al., 2014
52	SD41-35	P_1s	94.12	3.24	0.52	-	-	-	−33.2	−24.3	−23.4	−189	0.960	3.369	1.829	Li et al., 2014
53	SD46-47	P_1s	92.97	3.90	0.78	-	-	-	−33.4	−24	−23.1	−191	0.949	3.171	1.609	Li et al., 2014
54	Y69	P_1s	93.51	4.10	0.88	-	-	-	−31.7	−25.1	−23.2	−180	0.945	3.127	1.539	Li et al., 2014
55	S22-15	P_2x	82.66	3.12	0.72	1.03	5.04	-	−32.5	−24.5	−26.4	−182	0.953	3.277	1.466	Liu et al., 2007
56	S33-18	P_2x	72.72	3.11	0.50	0.75	16.94	-	−34.9	−24.5	−25.9	−185	0.950	3.152	1.828	Liu et al., 2007
57	S35-17	P_2x	90.44	4.60	0.79	1.14	1.94	-	−35.1	−24.2	−25.2	−187	0.941	2.979	1.762	Liu et al., 2007
58	S13-16	P_2x	89.90	4.67	0.87	1.43	1.92	-	−32.6	−25.6	−23.5	−186	0.939	2.958	1.680	Liu et al., 2007
59	S38-16	P_1s	89.96	4.64	0.96	2.01	1.27	-	−35.6	−25.8	−25.5	−188	0.940	2.965	1.576	Liu et al., 2009
60	S38-14	P_1s	89.33	5.87	1.23	1.03	1.18	-	−35.6	−25.2	−25.3	−190	0.924	2.722	1.563	Liu et al., 2009
61	S14-11-09	P_2x	92.52	3.78	0.75	1.18	1.10	-	−31.6	−24.0	−24.2	−172	0.950	3.198	1.617	Yu et al., 2013
62	S11-18-36	P_2x	90.16	5.50	1.15	1.47	0.94	-	−33.0	−23.3	−22.3	−180	0.927	2.797	1.565	Yu et al., 2013
63	S76-1-4	P_1s	90.38	6.03	1.18	0.82	0.71	-	−32.7	−23.6	−22.9	−182	0.922	2.707	1.631	Yu et al., 2013
64	S21	P_1s–P_2x	92.39	4.48	0.83	0.99	0.68	-	−33.4	−23.4	−23.8	−194	0.943	3.026	1.686	Dai et al., 2014
65	S48-14-76	P_1s–P_2x	92.73	3.48	0.65	1.47	1.14	-	−33.5	−22.8	−24.2	−192	0.955	3.283	1.678	Dai et al., 2014
66	S53	P_1s–P_2x	86.05	8.36	2.17	1.13	0.72	-	−35.6	−25.3	−23.7	−202	0.884	2.331	1.349	Dai et al., 2014
67	S53-78-46H	P_1s–P_2x	89.82	6.21	1.24	0.93	0.87	-	−33.9	−23.9	−23.0	−198	0.919	2.672	1.611	Dai et al., 2014
68	S76	P_1s–P_2x	86.41	8.37	2.33	0.13	1.21	-	−35.1	−24.6	−24.4	−203	0.882	2.334	1.279	Dai et al., 2014

(*continued on next page*)

Table 1 (*continued*)

Number	Well	Reservoir	Composition, %						$\delta^{13}C$, ‰			δD_1, ‰	C_1/C_{1-5}	$\ln(C_1/C_2)$	$\ln(C_2/C_3)$	Data sources
			CH_4	C_2H_6	C_3H_8	CO_2	N_2	H_2S	CH_4	C_2H_6	C_3H_8					
69	Z61	P_1s	88.98	6.83	1.53	0.55	0.85	-	−33.2	−23.5	−23.3	−194	0.908	2.567	1.496	Dai et al., 2014
70	S33-18	C–P	86.20	4.21	0.86	-	-	-	−31.7	−23.1	−23.4	−190	0.942	3.019	1.584	Cai et al., 2005
71	S40-16	C–P	88.40	5.60	1.16	-	-	-	−30.2	−27.2	−25.5	−198	0.925	2.759	1.574	Cai et al., 2005

Note: "-" represents no data.

Table 2
$\delta^{34}S$ data of H_2S, sulfur, pyrite, and anhydrite from subsalt strata of the Majiagou Formation in the Ordos Basin.

Number	Well	Sample	Stratum	$\delta^{34}S$, ‰	Data sources
1	L108	H_2S	$O_1m^{5(6)}$	22.6	Kong et al., 2024
2	T75	H_2S	$O_1m^{5(7)}$	21.9	Kong et al., 2024
3	T74	H_2S	$O_1m^{5(7)}$	20.1	Kong et al., 2024
4	T58	H_2S	$O_1m^{5(7)}$	23.3	Kong et al., 2024
5	JTA1	H_2S	$O_1m^{5(9)}$	24.6	Kong et al., 2024
6	TA38	H_2S	$O_1m^{5(9–10)}$	23.5	Kong et al., 2024
7	JT1	Sulfur	$O_1m^{5(7)}$	24.1	This study
8	JT1	Sulfur	$O_1m^{5(7)}$	23.6	This study
9	JT1	Sulfur	$O_1m^{5(7)}$	20.7	This study
10	JT1	Sulfur	$O_1m^{5(7)}$	23.1	This study
11	JT1	Sulfur	$O_1m^{5(7)}$	22.9	This study
12	JT1	Sulfur	$O_1m^{5(7)}$	23.3	This study
13	T112	Sulfur	$O_1m^{5(10)}$	23.2	This study
14	T112	Sulfur	$O_1m^{5(10)}$	24.2	This study
15	T112	Sulfur	$O_1m^{5(10)}$	24.8	This study
16	T112	Sulfur	$O_1m^{5(10)}$	23.9	This study
17	T112	Sulfur	$O_1m^{5(10)}$	22.5	This study
18	T112	Pyrite	$O_1m^{5(6)}$	4.9	Li et al., 2021
19	T112	Pyrite	$O_1m^{5(6)}$	5.9	Li et al., 2021
20	T112	Pyrite	$O_1m^{5(6)}$	5.5	Li et al., 2021
21	T112	Pyrite	$O_1m^{5(6)}$	7.4	Li et al., 2021
22	T112	Pyrite	$O_1m^{5(6)}$	4.3	Li et al., 2021
23	T112	Pyrite	$O_1m^{5(6)}$	9.4	Li et al., 2021
24	T112	Pyrite	$O_1m^{5(6)}$	8.9	Li et al., 2021
25	T112	Pyrite	$O_1m^{5(6)}$	8.7	Li et al., 2021
26	J9	Anhydrite	$O_1m^{5(6)}$	26.0	Kong et al., 2024
27	J11	Anhydrite	$O_1m^{5(6)}$	25.8	Kong et al., 2024
28	J2	Anhydrite	$O_1m^{5(6)}$	25.8	Kong et al., 2024
29	SH446	Anhydrite	$O_1m^{5(6)}$	26.9	Kong et al., 2024
30	JT1	Anhydrite	$O_1m^{5(6)}$	25.6	This study
31	JT1	Anhydrite	$O_1m^{5(6)}$	25.9	This study
32	JT1	Anhydrite	$O_1m^{5(7)}$	26.5	This study
33	T112	Anhydrite	$O_1m^{5(6)}$	27.4	This study
34	T112	Anhydrite	$O_1m^{5(6)}$	27.1	This study
35	T112	Anhydrite	$O_1m^{5(7)}$	27.3	This study

(between 0.80 and 0.85), likely due to low maturity (Fig. 2(b)). By contrast, C_1/C_{1-5} values for most of the other subsalt gases exceed 0.95, higher than those of the Upper Paleozoic gases (Fig. 2(b)). Unlike the decrease in C_2 with increasing C_1 content observed for the Upper Paleozoic gases (which have a single source and are mainly affected by thermal maturity), no similar relationship between the C_1 and C_2 contents was observed for the subsalt gas samples (Fig. 2(a)). Moreover, compared to the increase in the C_1/C_{1-5} value with increasing C_1 content and carbon isotope composition ($\delta^{13}C_1$) for the Upper Paleozoic gases, the C_1/C_{1-5} values of subsalt gases exhibited no positive relationship with C_1 content and $\delta^{13}C_1$ value (Fig. 2(b) and (c)). Thus, these results suggest that secondary alteration or multi-source mixing had likely occurred for the subsalt gases in the Majiagou Formation.

Additionally, the non-hydrocarbon components of the subsalt gases primarily consisted of CO_2, N_2, and H_2S, ranging from 0.07% to 33.79% (average: 5.65%; 34 samples), 0.67% to 67.01% (average: 12.72%; 35 samples), and 1.27% to 23.58% (average: 10.36%; 9 samples), respectively. These contents are higher than those of the Upper Paleozoic gases, whose non-hydrocarbon components primarily include CO_2 (0.01%–2.01%) and N_2 (0.68%–16.94%) (Table 1). This indicates that either the source of the subsalt gases differs from that of the Upper Paleozoic gases or the subsalt gases underwent TSR, increasing their CO_2 and H_2S contents. Moreover, previous studies reported that H_2S content of >5% in natural gas is commonly due to TSR (Liu et al., 2014a; Zhu et al., 2014); therefore, H_2S content exceeding 20% indicates the occurrence of TSR in the subsalt reservoirs.

In general, coal-type and oil-type gases can be distinguished by their $\delta^{13}C_2$ values, which are higher than −28.0‰ for gases derived from coal-bearing source rocks but lower than this value for oil-type gases (Dai, 1993). The $\delta^{13}C_2$ values of the Upper Paleozoic gases ranged from −27.2‰ to −20.8‰ (Fig. 2(d) and Table 1), indicating that their correct classification as coal-type gas. By contrast, the $\delta^{13}C_2$ values of the subsalt gases varied widely, ranging between −34.7‰ and −19.1‰ (Fig. 2(d) and Table 1), further suggesting that their source is a mixture of coal-type and oil-type gases, or the result of TSR reformation of oil-type gases,

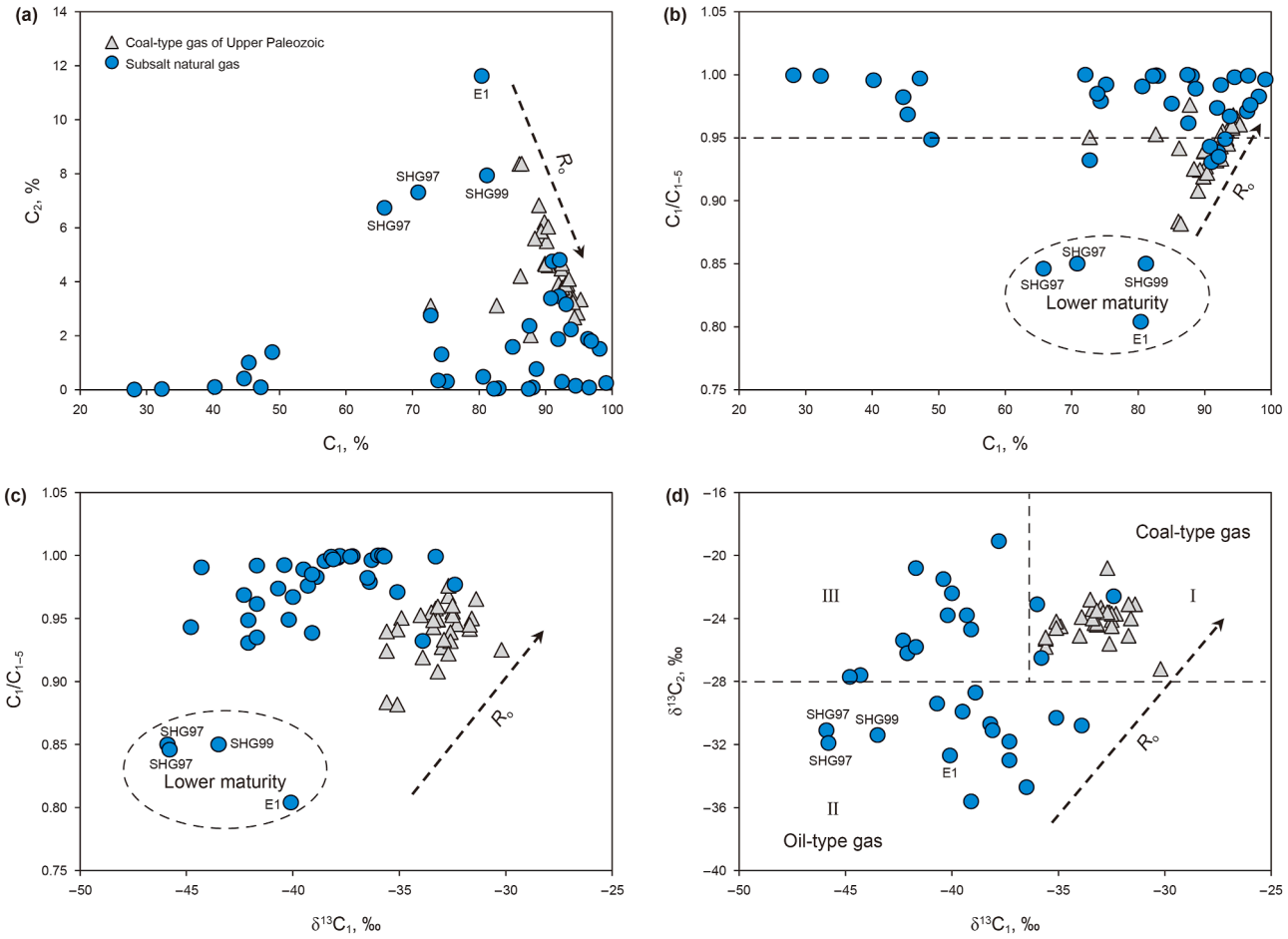

Fig. 2. Geochemical variations of the subsalt gases from the Majiagou Formation and of the Upper Paleozoic gases in the Ordos Basin. **(a)** C_2 contents and **(b)** C_1/C_{1-5} ratios versus C_1 contents, and **(c)** C_1/C_{1-5} ratios and **(d)** $\delta^{13}C_2$ values versus $\delta^{13}C_1$ values. Data on the natural gas sources are listed in Table 1.

which leads to increased $\delta^{13}C_2$ values (Guo et al., 2022a, 2022b; Liu et al., 2019; Yang et al., 2022). The $\delta^{13}C_1$ values of the subsalt gases were basically lower than those of the Upper Paleozoic gases classified as coal-type gas within region I in Fig. 2(d). The $\delta^{13}C_1$ and $\delta^{13}C_2$ values combined indicate that the subsalt gases within region II in Fig. 2(d) should be classified into oil-type gas. However, the source of the subsalt gases within region III in Fig. 2(d) remains unknown, because their formation could result from the mixing between coal-type and oil-type gases and from TSR alteration of oil-type gases. Furthermore, it can be concluded that the lowest C_1 contents and C_1/C_{1-5} values of the four subsalt gas samples from E1, SHG97, and SHG99 wells within region II in Fig. 2(d) are determined by their lower maturity, as reflected by their low $\delta^{13}C_1$ values (most less than −40.0‰, Table 1). This was also confirmed by the range of R_o values (1.2%–1.6%) of the Majiagou Formation in the area of these wells (Fig. 1(a)).

The primary and secondary gases from oil- and gas-prone kerogen can be distinguished based on their variation in $\ln(C_1/C_2)$ and $\ln(C_2/C_3)$ (Prinzhofer and Huc, 1995). Furthermore, the TSR transformation characteristics of natural gas can be determined, because TSR causes the $\ln(C_2/C_3)$ to first increase and then decrease with increasing $\ln(C_1/C_2)$ (Guo et al., 2022b). With increasing $\ln(C_1/C_2)$ values (mainly <4.0), the $\ln(C_2/C_3)$ value of the Upper Paleozoic gases showed an upward trend and fell between the $\ln(C_2/C_3)$ values of secondary cracking for type II and type III kerogen (Fig. 3), indicating that the Upper Paleozoic gases primarily originated from the secondary cracking of mixed organic matter in coal-bearing source rocks. However, for the subsalt gases, the $\ln(C_2/C_3)$ value demonstrated an upward trend with increasing $\ln(C_1/C_2)$ values (<4.0) but a downward trend when $\ln(C_1/C_2)$ values exceeding 4.0 (Fig. 3), suggesting that these gases primarily originated from secondary cracking of organic matter and had undergone TSR. Additionally, unlike the variation caused by secondary cracking, the $\ln(C_1/C_2)$ values of the subsalt gases increase abnormally (Fig. 3), suggesting that much more C_2 was consumed during the TSR process.

The effects of TSR on hydrocarbon compositions are selective at different maturity stages under practical geological conditions. For example, the C_{2-5} compounds are preferentially oxidized in the gas hydrocarbon stage because methane has the highest thermal stability, whereas the gasoline fraction is firstly oxidized during the liquid hydrocarbon stage (Guo et al., 2022a, 2022b; Heydari and Moore, 1989; Liu et al., 2006, 2014b; Orr, 1990). Consequently, the TSR reaction would result in an abnormal increase in the C_1/C_{1-5} ratio of natural gas. Thus, for the subsalt gases of the Majiagou Formation, an abnormal increase in the C_1/C_{1-5} ratio is likely caused by TSR. The TSR of natural gas can also increase the $\delta^{13}C$ value of the C_{2-5} compounds, as thermal stability of the ^{13}C-related C–C bond is higher than that of the ^{12}C-related C–C bond. This is likely the key reason for the abnormally high $\delta^{13}C_2$ values observed

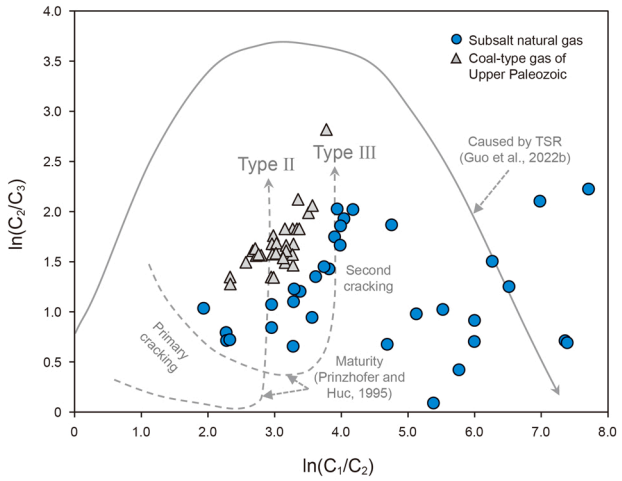

Fig. 3. Relationship between the $\ln(C_1/C_2)$ and $\ln(C_2/C_3)$ values of the subsalt gases in the Majiagou Formation and the Upper Paleozoic gases in the Ordos Basin. Modified after Guo et al. (2022b) and Prinzhofer and Huc (1995). Data on the natural gas sources are listed in Table 1.

for some subsalt gases of the Majiagou Formation. Therefore, unlike the Upper Paleozoic coal-type gases, which are influenced solely by their maturity, identifying the subsalt gas source becomes more difficult because TSR affects its carbon isotope composition. In particular, the effects of TSR on C_{2+} compounds may lead to incorrect source identification when relying solely on $\delta^{13}C_{2+}$ values.

4.2. Source of the subsalt natural gas

The $\delta^{13}C_2$ values of the H_2S-containing natural gas from the subsalt reservoirs exhibited an increasing trend with an increase in the H_2S content (Fig. 4(a)). An important reason for the heavy carbon isotope composition of ethane in the subsalt gases is TSR, particularly in natural gas with lower thermal maturity (equivalent R_o <1.5%) (Yang et al., 2022). Consequently, with the positive shift in $\delta^{13}C_2$ caused by the TSR reaction, this parameter becomes ineffective for identifying the gas source (Cai and Wang, 2024). The $\delta^{13}C_2$ values of the subsalt gases gradually increased from less than −30‰ to over −24‰ under TSR action (Fig. 4(a)), resulting in some oil-type gases exhibiting the characteristic of coal-type gas in terms of $\delta^{13}C_2$ value. This further confirms that the $\delta^{13}C_2$ parameter cannot be used to determine the source of subsalt gases from the Majiagou Formation in the Ordos Basin.

Methane can only be oxidized at the last stage of TSR because its thermal stability higher that of other hydrocarbon gas compounds (Cai et al., 2003, 2004, 2013; Guo et al., 2022a, 2022b; Hao et al., 2008; Li et al., 2019; Liu et al., 2006). Although methane may be generated when C_{2+} gaseous hydrocarbon components are oxidized by TSR, the slight variations in methane caused by these reactions would be diluted owing to the high proportion of thermogenic methane in natural gas. Additionally, the $\delta^{13}C_2$ value increases rapidly, whereas the $\delta^{13}C_1$ value remains unaffected, at the C_{2+} gaseous hydrocarbon-dominated TSR stage. Conversely, the $\delta^{13}C_1$ value increases, but the $\delta^{13}C_2$ value remains relatively constant, at the methane-dominated TSR stage (Hao et al., 2008). The $\delta^{13}C_2$ value of the subsalt gases had an obvious positive relationship with the H_2S content, whereas no relationship was observed between the $\delta^{13}C_1$ value and H_2S content (Yang et al., 2022), indicating that the TSR modification of the subsalt gases occurs mainly at the C_{2+} gaseous hydrocarbon-dominated stage. Accordingly, we speculated that the isotope composition of methane is weakly affected by TSR and can be used to effectively identify the source of the subsalt gases in the Majiagou Formation. The $\delta^{13}C_1$ values of the subsalt gases ranged from −45.9‰ to −32.4‰ (average: −39.2‰), significantly lower than those of the coal-type gases from the Upper Paleozoic, which ranged from −35.6‰ to −30.2‰ (average: −33.2‰) (Fig. 5 and Table 1). This suggests that the source of the subsalt gases is different from that of coal-type gas and can therefore be primarily classified as oil-type gas. The hydrogen isotope composition of methane (δD_1) is an effective indicator in distinguishing marine oil-type gas from coal-type gas, as the δD_1 value of marine oil-type gas is higher than that of coal-type gas under similar thermal maturity (Wang et al., 2015). Thus, by combining this parameter with the $\delta^{13}C_1$ value, marine oil-type gas can be effectively distinguished from coal-type gas. In this study, the δD_1 values of the subsalt gases were higher than those of the Upper Paleozoic coal-type gases, reflecting the characteristics of marine oil-type gas (Fig. 4(b)). Therefore, the subsalt gases of the Majiagou Formation have been revealed to

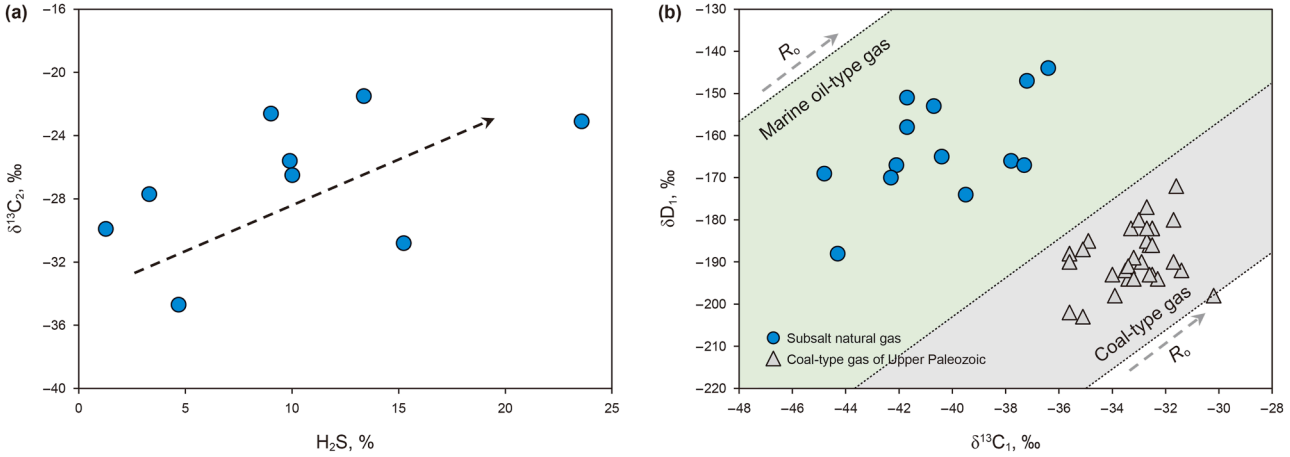

Fig. 4. **(a)** Variation characteristics of the $\delta^{13}C_2$ value with increasing H_2S content for the subsalt gases of the Majiagou Formation, **(b)** the relationship between the $\delta^{13}C_1$ and δD_1 values of the subsalt gases from the Majiagou Formation and the Upper Paleozoic gases in the Ordos Basin. Data on the natural gas sources are listed in Table 1. The plate of Fig. 4(b) is modified after Wang et al. (2015).

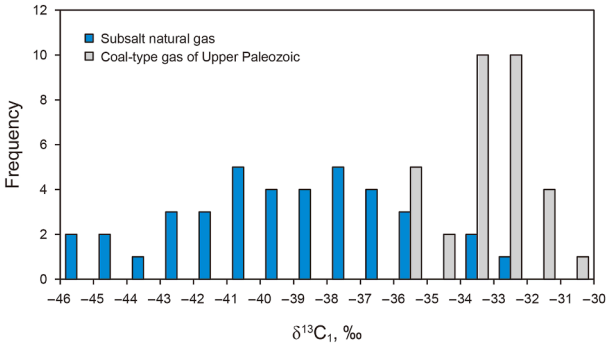

Fig. 5. Distribution of the $\delta^{13}C_1$ value of the subsalt gases from the Majiagou Formation and those of the Upper Paleozoic gases in the Ordos Basin. Data on the natural gas sources are listed in Table 1.

be derived mainly from the source rocks of the Lower Paleozoic, belonging to typical marine oil-type gas.

The $\delta^{13}C_1$ value can be used to evaluate the thermal maturity of natural gas because it would increase with the thermal evolution. Furthermore, the R_o value of natural gas can be calculated from the $\delta^{13}C_1$ value, with the formula for the oil-type gas being $\delta^{13}C_1 = 27.55\lg(R_o) - 47.22$ (Zhao and Liu, 2008). The $\delta^{13}C_1$ values of the subsalt gases exhibited an increasing trend with an increase in R_o of the Ordovician top surface (Fig. 6(a)). Furthermore, the R_o values calculated from the $\delta^{13}C_1$ values were equivalent to or slightly higher than the R_o of the Ordovician top surface (Fig. 6(b)), confirming that the carbon isotope composition of methane is either weakly affected or unaffected by TSR. Six subsalt gas samples from the O_1m^5 reservoir abnormally displayed $\delta^{13}C_1$ values higher than −36.0‰ (Table 1), suggesting that they were likely influenced by TSR because gypsum–salt rocks were more developed in this interval and promoted the TSR reaction (Fig. 1(b)). However, the $\delta^{13}C_1$ value is still considered an effective indicator of gas sources as it is rarely affected by TSR and would not cause identification errors compared with the changes in the $\delta^{13}C_2$ value.

Considering the noteworthy TSR-mediated modification in the carbon isotope composition of ethane, the $\delta^{13}C_1$ and δD_1 parameters should be selected for identifying the source of the subsalt gases. In conclusion, the subsalt gases of the Majiagou Formation in the Ordos Basin primarily originated from the marine source rocks in the Lower Paleozoic and are classified as oil-type gas. That is, the subsalt gases belong to self-generated and self-stored natural gas.

4.3. Characteristics of secondary minerals in the subsalt reservoir

The cracks and caves in the subsalt reservoirs of the Majiagou Formation are widely filled by secondary calcite and elemental sulfur. Furthermore, these secondary calcite and sulfur often coexisted and bitumen impregnations are commonly seen (Fig. 7). TSR is a thermodynamically driven chemical reaction in which sulfates are reduced, and hydrocarbons are oxidized. The reaction can be divided into three stages based on the composition of hydrocarbon reactants, with the equations expressed as follows (Hao et al., 2008; Machel et al., 1995; Worden and Smalley, 1996):

Liquid hydrocarbon as the main reductant:

$$\text{Hydrocarbon} + SO_4^{2-} \rightarrow \text{altered hydrocarbons} + \text{bitumen} + H_2S + CO_2 \quad (1)$$

C_{2+} hydrocarbon gas as the main reductant:

$$C_nH_{2n+2} + nCaSO_4 \rightarrow nCaCO_3 + H_2S + (n-1)S + nH_2O \quad (2)$$

Methane as the main reductant:

$$CH_4 + CaSO_4 \rightarrow CaCO_3 + H_2S + H_2O \quad (3)$$

Obviously, TSR in the reservoir generates an abundance of bitumen at the liquid hydrocarbon stage, and elemental sulfur is easily formed by the TSR reaction involving C_{2-5} gaseous hydrocarbons. However, calcite is likely found at any stage of TSR because CO_2 is always formed during this reaction process. Therefore, we can conclude that the formation of calcite and elemental sulfur in the cracks and caves of the subsalt reservoirs is likely related to sulfate reduction coupled with oxidation of the C_{2-5} gaseous hydrocarbons.

In the reservoir, no bitumen or only trace amounts of it formed if gaseous hydrocarbons participated in the TSR reaction (King et al., 2014). Thus, the bitumen impregnations in some of the

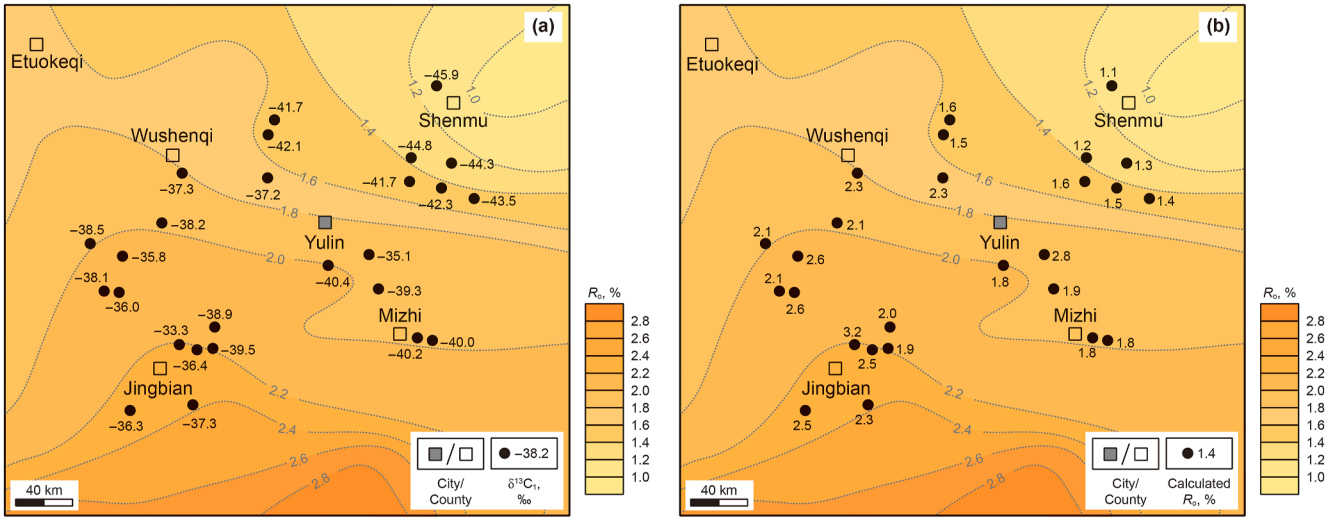

Fig. 6. Variation characteristics of the $\delta^{13}C_1$ **(a)** and calculated R_o **(b)** values for the subsalt gases of the Majiagou Formation in the Ordos Basin and their relationship with the R_o of the Ordovician top surface. The locations of natural gas wells are indicated by the green wells in Fig. 1(a).

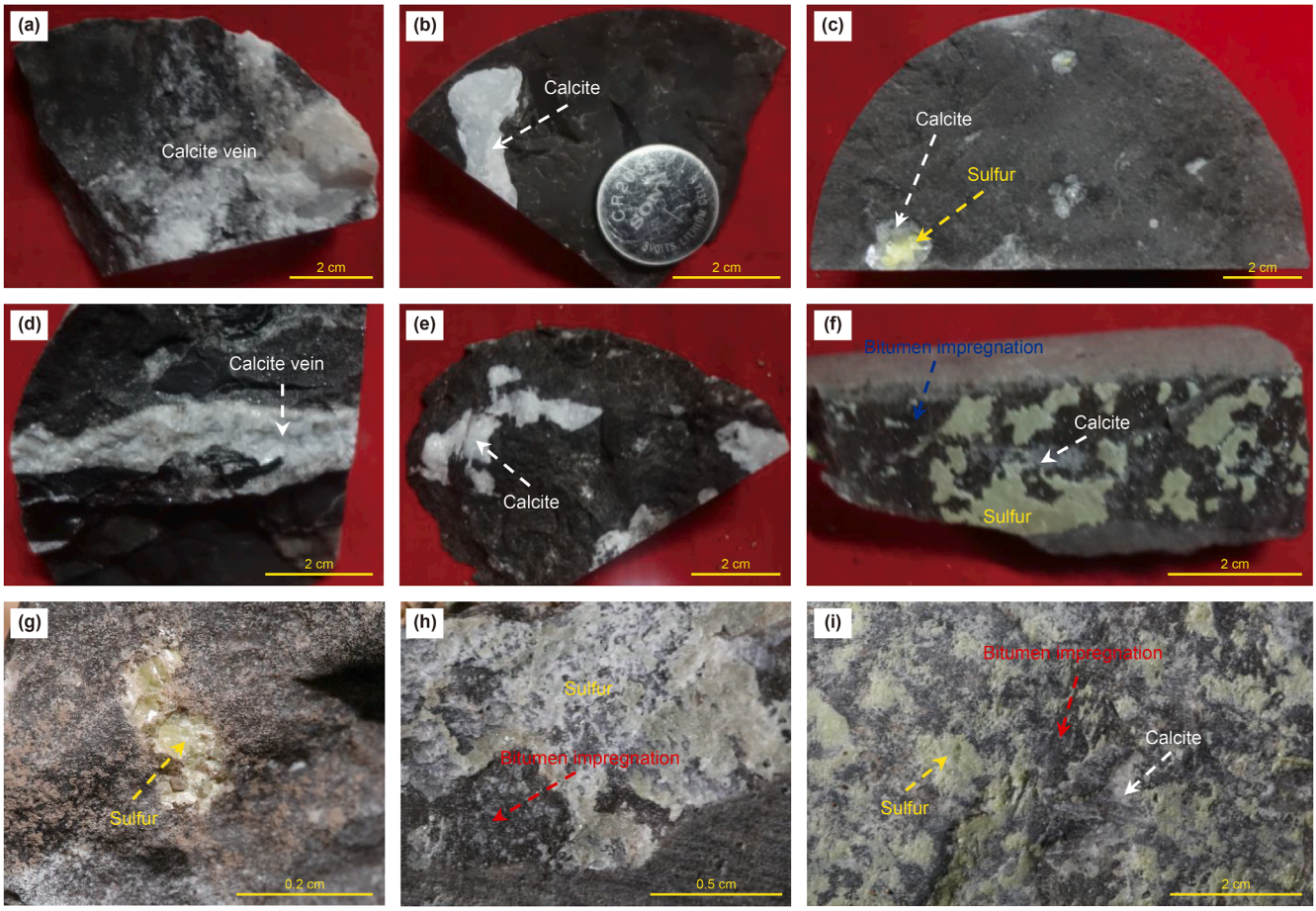

Fig. 7. Characteristics of secondary minerals in drilling cores from the subsalt reservoirs of the Majiagou Formation in the Ordos Basin. The locations of the sampling wells are shown in Fig. 1(a). **(a)** TA112, 3333.89 m, $O_1m^{5(6)}$, calcite vein in the dolomite crack; **(b)** TA112, 3522.17 m, O_1m^4, calcite in the limestone cave; **(c)** TA112, 3582.57 m, O_1m^4, calcite and sulfur coexisting in the limestone cave; **(d)** TA112, 3316.77 m, $O_1m^{5(6)}$, calcite vein in the dolomite crack; **(e)** TA112, 3382.05 m, $O_1m^{5(6)}$, calcite in the dolomite cave; **(f)** TA112, 3510.14 m, $O_1m^{5(10)}$, sulfur associated calcite and bitumen impregnation in the dolomite crack; **(g)** JT1, 3668.6 m, $O_1m^{5(7)}$, sulfur in the dolomite cave; **(h)** JT1, 3668.64 m, $O_1m^{5(7)}$, sulfur associated bitumen impregnation in the dolomite crack; **(i)** JT1, 3628.4 m, $O_1m^{5(6)}$, sulfur associated calcite and bitumen impregnation in the dolomite crack.

cracks of the subsalt reservoir are likely related to the TSR of natural gas. On the one hand, trace amounts of bitumen possibly formed through the TSR of gaseous hydrocarbons. On the other hand, a small amount of bitumen was formed by TSR of the trace amounts of light hydrocarbons carried in the subsalt natural gas. In this process, H_2S likely initiated sulfate reduction because this reaction pathway of TSR is easier. This reaction involves labile organosulfur compounds (LSCs) and is divided into two steps (Cai et al., 2022): (i) the formation of LSCs by the reaction of H_2S reaction with the trace amounts of light hydrocarbons in the subsalt gases according to Equation (4), and (ii) sulfate reduction coupled with oxidation of the LSCs and light hydrocarbons according to Equation (5).

$$H_2S + \text{hydrocarbon} \rightarrow \text{LSCs} \quad (4)$$

$$\text{LSCs} + MgSO_4 + \text{hydrocarbons} \rightarrow \text{OSCs} + \text{O-bearing compounds} + \text{bitumen} + H_2S + CO_2 + Mg^{2+} \quad (5)$$

Compared with the $\delta^{13}C$ values of primary carbonate rocks, those of TSR-related calcites exhibit a significant negative offset because of the conversion of organic carbon to inorganic carbon (Worden and Smalley, 1996). The $\delta^{13}C$ values of the secondary calcites in the TA112 subsalt reservoir ranged from −21.1‰ to −4.4‰ (average: −10.4‰) and were significantly lower than those of the primary dolomite, which exhibited values ranging from −2.5‰ to 1.2‰ (Fig. 8(a)). This indicates that these secondary calcites in the cracks and caves of the subsalt reservoirs were primarily formed by TSR reactions. Additionally, the associated elemental sulfur had $\delta^{34}S$ values ranging from 22.5‰ to 24.8‰, close to those of the anhydrite in the Majiagou Formation (25.6‰–27.4‰) (Table 2). This further suggests that they are TSR-related calcite, as no significant sulfur isotopic fractionation (mostly −1‰ to −3‰) occurs during the TSR process (Cai et al., 2022). The fluid inclusions in the secondary calcites of the TA112 subsalt reservoir had abundant H_2S and formed at 160–220 °C (Wu et al., 2022), confirming our speculation that the secondary calcites filling the cracks and caves of the subsalt reservoir are primarily caused by TSR.

Generally, the $\delta^{34}S$ values of the H_2S and elemental sulfur generated by TSR would cause a negative offset compared with the $\delta^{34}S$ value of sulfate due to isotopic kinetic fractionation, the value of which is typically less than 15‰ (mostly at 1‰–3‰) (Cai et al., 2022; Zhu et al., 2014). The $\delta^{34}S$ values of H_2S and elemental sulfur ranged from 20.1‰ to 24.6‰ and 20.7‰ to 24.8‰, respectively (Fig. 8(b) and Table 2). Compared with the $\delta^{34}S$ value of anhydrite

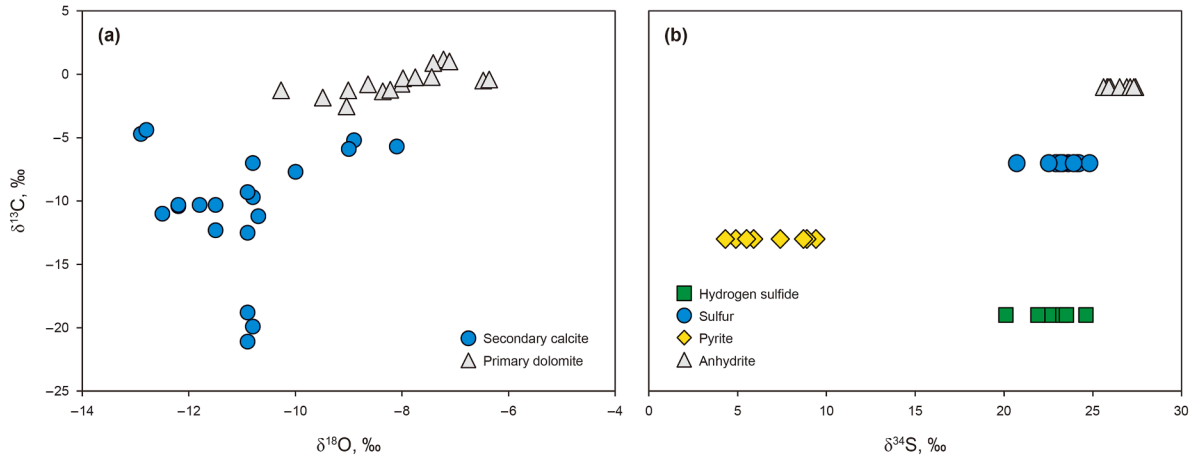

Fig. 8. **(a)** Variation characteristics of the $\delta^{13}C$ and $\delta^{18}O$ values for the secondary calcite in the subsalt crack and caves, as well as the primary dolomite of the TA112 well; **(b)** $\delta^{34}S$ distribution characteristics of H_2S, elemental sulfur, pyrite, and anhydrite from the subsalt reservoirs of the Majiagou Formation in the Ordos Basin. The $\delta^{13}C$ and $\delta^{18}O$ values for the subsalt carbonates are from Li et al. (2021) and the $\delta^{34}S$ data sources are listed in Table 2.

(average: 26.4‰, range: 25.6‰–27.4‰), those of H_2S and elemental sulfur caused an average negative offset of 3.7‰ and 3.1‰, respectively, indicating that the H_2S and elemental sulfur in the subsalt reservoirs were primarily formed by the TSR reaction. Thus, the rich TSR-related elemental sulfur confirmed the results of gas geochemical and mineralogical analyses; that is, the C_{2-5} gaseous hydrocarbons are the primary reductants for the TSR reaction in the subsalt reservoirs of the Majiagou Formation.

According to Equations (1)–(5), H_2S is an important product of the TSR reaction. However, it dissolves easily in the stratigraphic water, resulting in its massive loss (Cai et al., 2013, 2015). Thus, this could be a reason for the wide variation in H_2S content in the

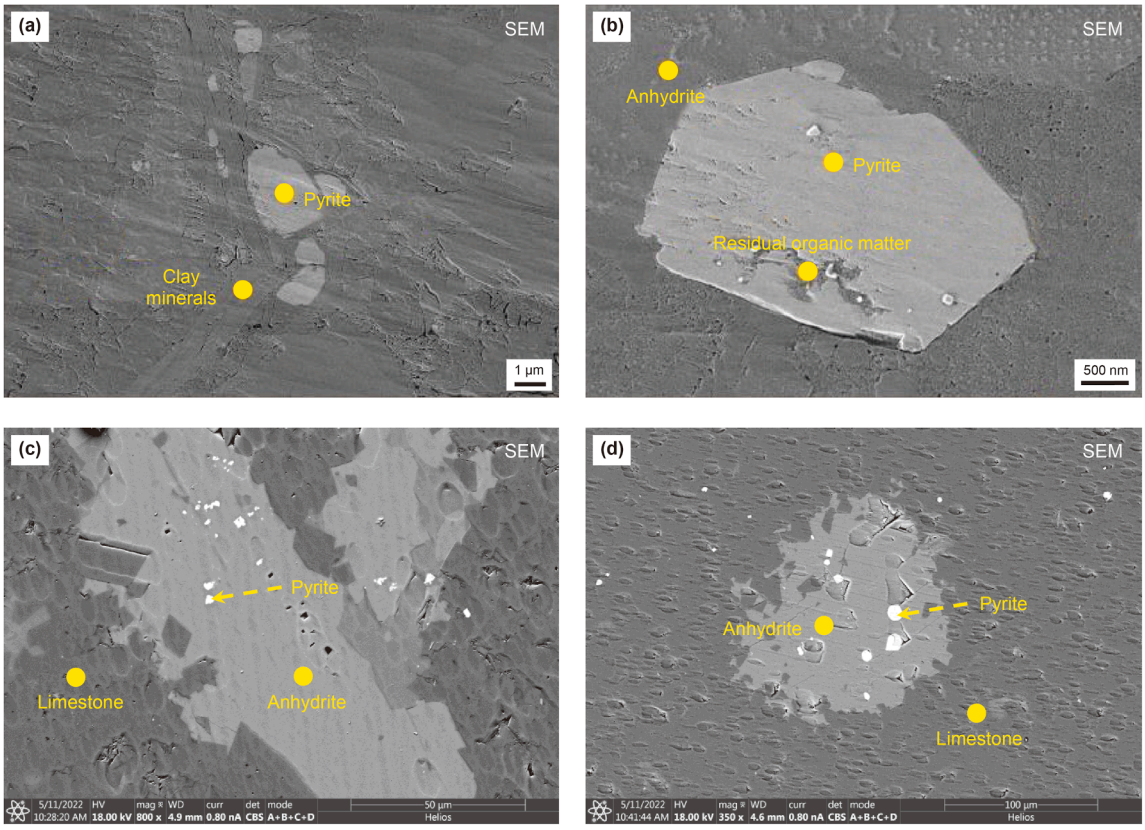

Fig. 9. SEM images showing the characteristics of pyrite in the subsalt carbonate rocks from the Majiagou Formation in the Ordos Basin. The locations of the sampling wells are shown in Fig. 1(a). **(a)** TA112, 3763.01 m, O_1m^3, pyrite filling pores of the clay minerals in the dolomite; **(b)** TA112, 3334.42 m, $O_1m^{5(6)}$, pyrite coexisting with residual organic matter in the dissolution pores of anhydrite; **(c–d)** JT1, 3757.27 m, O_1m^4, pyrite filling dissolution pores of anhydrite nodules in the limestone. Data of (a) and (b) are from Li et al. (2021).

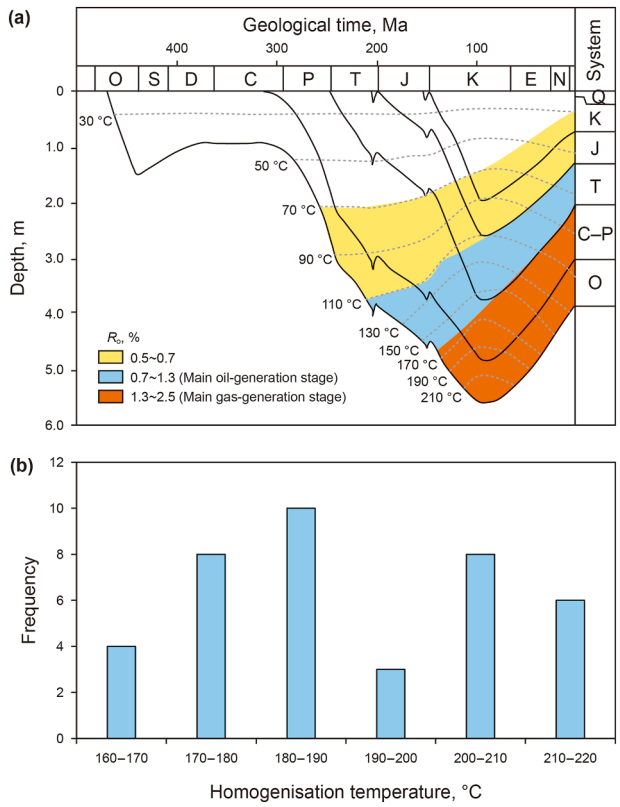

Fig. 10. **(a)** Burial–thermal history of the TA112 well modified according to Wu et al. (2022), and **(b)** homogenisation temperatures collected from Wu et al. (2022), displaying the trapping temperatures of aqueous inclusions co-captured with CH_4- and H_2S-containing inclusions in secondary calcites. The location of the TA112 well is shown in Fig. 1(a).

subsalt gases. Furthermore, excessive H_2S can reduce trivalent iron (Fe^{3+}) in the stratigraphic water to form pyrite (FeS_2) according to the following two equations (Rickard, 1997):

$$2Fe^{3+} + 3H_2S \rightarrow 2FeS + S + 6H^+ \quad (6)$$

$$FeS + H_2S \rightarrow FeS_2 + H_2 \quad (7)$$

This reaction process is likely another reason for the wide variation in the H_2S content of the subsalt gases in the Majiagou Formation. The pores of clay minerals or the pores of anhydrite nodules and their adjacent carbonates were filled with many euhedral or subhedral pyrites, with some of the pyrite aggregates comprising residual organic matter (Fig. 9), suggesting that pyrite formation in the subsalt reservoirs was likely caused by TSR. Additionally, the $\delta^{34}S$ values of the pyrites ranged from 4.3‰ to 9.4‰, significantly less than the $\delta^{34}S$ values of H_2S (Fig. 8(b) and Table 2), which further suggests that the pyrites from the subsalt reservoirs are related to the TSR reaction because pyrite formation would result in further sulfur isotope fractionation according to Equations (6) and (7).

Consequently, based on their occurrence as well as the carbon and sulfur isotope analyses, the calcite and elemental sulfur filling the cracks and caves of the subsalt reservoirs can be considered as TSR-related products. Furthermore, we can conclude that gaseous hydrocarbons are the main reductant of TSR owing to the rich TSR-related elemental sulfur and a small amount of bitumen in the subsalt reservoirs. Except for the amount lost to dissolution, TSR-related pyrite formation is an important reason for the wide variation in H_2S content and even for non-detectable in the subsalt reservoirs of the Majiagou Formation in the Ordos Basin.

4.4. Accumulation characteristics of the subsalt natural gas

Fluid charging history can be studied through homogenisation temperature of fluid inclusions and basin modelling (Arouri et al., 2010; Hu et al., 2010; Tian et al., 2014; Wang et al., 2016). The trapping temperature is recorded by the homogenisation temperature of fluid inclusions (Goldstein, 2001), and co-captured aqueous inclusions are better than hydrocarbon inclusions in estimating oil trapping temperature (Arouri et al., 2010; Munz, 2001). Therefore, as shown in Fig. 10, the one-dimensional burial–thermal history of the TA112 well was modified according to Wu et al. (2022), and the homogenisation temperatures of aqueous inclusions co-captured with hydrocarbon- and H_2S-containing inclusions in the secondary calcites of the TA112 well were collected.

The main oil-generating stage of the Ordovician source rocks occurred at the Jurassic period (~200–150 Ma), whereas the main gas-generating stage started at the Early Cretaceous and ended when the basin experienced continuous uplift from the Late

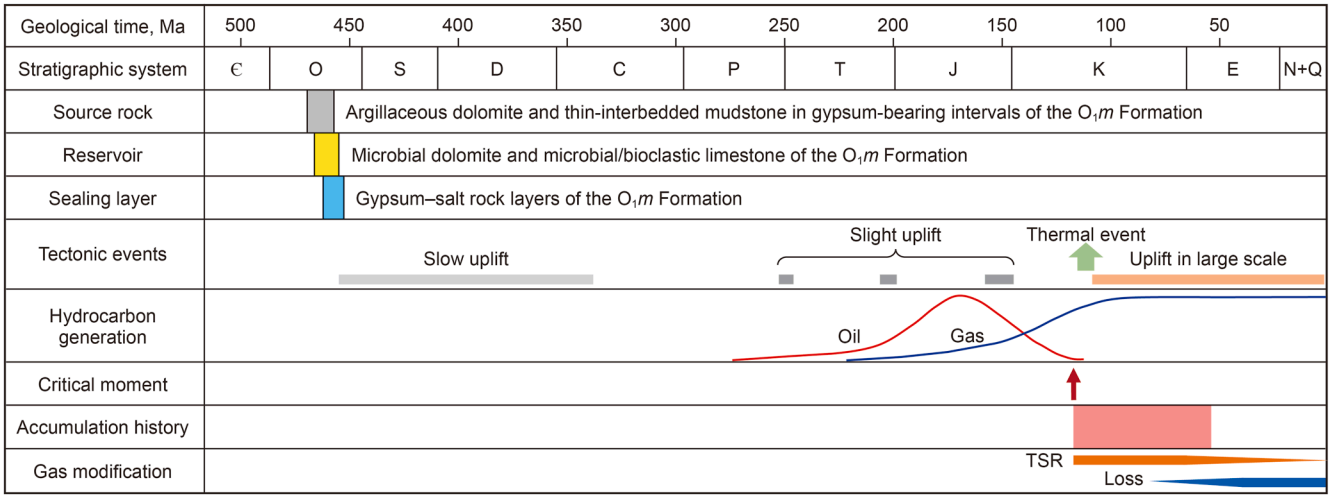

Fig. 11. Event chart showing major elements of the petroleum system and gas accumulation and reconstruction in the subsalt reservoirs of the Majiagou Formation in the Ordos Basin.

Cretaceous based on the burial–thermal history of the TA112 well (Fig. 10(a)). Thus, the Ordovician strata of the TA112 well experienced a maximum temperature of approximately 210–220 °C at circa 95 Ma. The homogenisation temperatures of the aqueous inclusions in the secondary calcites of the TA112 well were primarily distributed between 160 and 220 °C (Fig. 10(b)), with the highest homogenisation temperature being equivalent to the maximum temperature that occurred in the Ordovician strata of the TA112 well. Furthermore, the homogenisation temperatures of the aqueous inclusions corresponded to the main gas-generating stage of the Ordovician source rocks, suggesting that hydrocarbon migration and accumulation occurred after the Early Cretaceous and through gaseous hydrocarbons.

The source rocks of the Majiagou Formation consist primarily of argillaceous dolomite and thin inter-bedded mudstone in the gypsum-bearing carbonate intervals, with the residual total organic carbon (TOC) ranging from 0.16% to 2.97% (average: 0.45%) (Kong et al., 2024). Microbial dolomite and microbial/bioclastic limestone are the primary reservoirs of the subsalt gases in the Majiagou Formation (Hu et al., 2022). Together with the gypsum–salt rocks, a good gas accumulation system had formed (Fig. 11). During the main oil-generating period, few hydrocarbons were expelled from the source rocks of the Majiagou Formation because of the insufficient driving force for their expulsion and the lack of a migration pathway. On one hand, the hydrocarbon-generating pressurisation of the Majiagou source rocks was limited because of their low TOC content, and the good sealing property of gypsum–salt rocks in the source rock intervals would effectively prevent macromolecule hydrocarbon migration. On the other hand, because of the weak tectonic activity and only slight uplift (Yang et al., 2024), the structural stress droved weakly and few structural fractures developed. However, during the main gas-generating period, large-scale uplift and a geothermal incident occurred in the Ordos Basin (Ren et al., 2021), which greatly promoted massive gaseous hydrocarbon generation and migration. Consequently, the subsalt gas reservoirs can be classified as primary natural gas accumulations. This confirms the previous conclusion that the major reductants of the TSR reaction in the subsalt reservoirs of the Majiagou Formation are gaseous hydrocarbons.

Although the strong uplift during the main gas-generating period can promote massive gas migration and accumulation, continuous uplift at a later period is adverse to gas preservation. Thus, the subsalt gas reservoirs in the Majiagou Formation were continuously being lost from the Late Cretaceous to the Quaternary period owing to the continuous uplift of the Ordos Basin, and the loss intensity gradually increased (Fig. 11). Aside from the natural gas loss caused by the tectonic uplift, the subsalt gas reservoirs in the Majiagou Formation constantly underwent TSR alteration, owing to an abundance of SO_4^{2-} supplied from the dissolution of anhydrite, meeting a necessary condition of TSR (Goldhaber and Orr, 1995; Zhang et al., 2008). However, the TSR alteration gradually weakened from the Paleogene because the formation temperature had decreased under the uplift of the Ordos Basin.

In summary, the subsalt gas reservoirs of the Majiagou Formation in the Ordos Basin primarily formed through the direct migration and accumulation of gaseous hydrocarbons and were unrelated to the cracking of paleo-oil reservoirs. Thus, in future explorations of these subsalt gases in this region, more focus should be placed on the geological conditions for hydrocarbon accumulation since the Cretaceous period, including tectonic activity, source–reservoir–cap assemblages, and gas migration. TSR alteration of the subsalt gas reservoirs is another key focus in gas accumulation studies, particularly in the identification of gas sources, because the TSR reaction would cause some modifications in the geochemical characteristics of natural gas.

5. Conclusions

The characteristics and sources of the natural gases accumulated in the Ordovician Majiagou Formation of the Ordos Basin were studied using geochemical analysis methods. The TSR was characterised through investigations of the secondary minerals in the subsalt reservoirs and their geochemical data. Furthermore, the effects of TSR on natural gas accumulation in the carbonate–evaporite assemblage were explored. The following conclusions are made.

(1) Many C_{2+} components were consumed by the TSR reaction. Consequently, the subsalt gases that underwent TSR alteration exhibited higher C_1/C_{1-5} and $\delta^{13}C_2$ values than those of the gases affected by thermal evolution only. In particular, for the subsalt reservoirs, the $\delta^{13}C_2$ values of some oil-type gases that underwent TSR alteration reflected the characteristics of coal-type gas.

(2) $\delta^{13}C_1$ and δD_1 values can be used to effectively identify the source of the subsalt gases in the Ordovician Majiagou Formation because TSR has the weakest influence on methane. Based on their lower $\delta^{13}C_1$ values and higher δD_1 values than those of the Upper Paleozoic coal-type gases, the Ordovician subsalt gases in the Ordos Basin were primarily derived from marine source rocks, belonging to self-generated and self-stored natural gas reservoirs.

(3) The cracks and caves of the Ordovician subsalt reservoirs in the Ordos Basin were commonly filled by secondary minerals related to the TSR reaction, including secondary calcite, elemental sulfur, and pyrite, but few bitumen co-existed with these secondary minerals. Combined with the results of gas geochemical analyses, these findings indicate that the major reductants of the TSR reaction were gaseous hydrocarbons, particularly the C_{2-5} components.

(4) The Ordovician subsalt gas reservoirs in the Ordos Basin primarily formed through the direct migration and accumulation of gaseous hydrocarbons. Moreover, they were unrelated to the cracking of paleo-oil reservoirs, because it is difficult for liquid hydrocarbons to be expelled from the low-TOC and gypsum–salt-rock-containing source rock layers in the Majiagou Formation. Therefore, future explorations of the Ordovician subsalt reservoirs in the Ordos Basin should focus on the primary gas reservoirs.

CRediT authorship contribution statement

Xiao-Yan Chen: Writing – original draft, Methodology, Conceptualization. **Wen-Hui Liu:** Project administration, Methodology, Conceptualization. **Hou-Yong Luo:** Data curation, Writing – review & editing. **Xiao-Feng Wang:** Formal analysis, Supervision. **Liu-Bin Wei:** Resources, Investigation. **Dong-Dong Zhang:** Validation, Writing – review & editing. **Wen Zhang:** Data curation. **Wen-Qing Wang:** Visualization.

Declaration of competing interest

The authors declare that they have no known competing financial interests or personal relationships that could have appeared to influence the work reported in this paper.

Acknowledgements

This study was financially supported by China Postdoctoral Science Foundation (Grant No. 2021M692608), National Natural Science Foundation of China (Grant Nos. 42172173, 42102172, 41930426, 42202186), Shaanxi Provincial Department of Education Youth Innovation Team Project (Grant No. 23JP173) and the PetroChina Changqing Oilfield Company, Science and Technology Major Project (Grant No. 2024D1JC06-03). The authors wish to thank the collaboration and support of the Exploration and Development Research Institute of PetroChina Changqing Oilfield Company. Four anonymous reviewers are greatly acknowledged for their constructive comments that substantially improved the quality of this manuscript.

References

Anisimov, L.A., 1978. Conditions of abiogenic reduction of sulfates in oil- and gas-bearing basins. Geochem. Int. 15, 6–70.

Arouri, K.R., Laer, P.J.V., Prudden, M.H., et al., 2010. Controls on hydrocarbon properties in a Paleozonic petroleum system in Saudi Arabia, exploration and development implications. AAPG (Am. Assoc. Pet. Geol.) Bull. 94 (2), 163–188. https://doi.org/10.1306/07060908133.

Cai, C., Amrani, A., Worden, R.H., et al., 2016. The sulfur isotopic compositions of individual sulfur compounds and their genetic link in the Lower Paleozoic petroleum pools of the Tarim Basin, NW China. Geochem. Cosmochim. Acta 182, 88–108. https://doi.org/10.1016/j.gca.2016.02.036.

Cai, C., He, W., Jiang, L., et al., 2014. Petrological and geochemical constraints on porosity difference between Lower Triassic sour- and sweet-gas carbonate reservoirs in the Sichuan Basin. Mar. Petrol. Geol. 56, 34–50. https://doi.org/10.1016/j.marpetgeo.2014.04.003.

Cai, C., Hu, G., He, H., et al., 2005. Geochemical characteristics and origin of natural gas and thermochemical sulphate reduction in Ordovician carbonates in the Ordos Basin, China. J. Petrol. Sci. Eng. 48 (3), 209–226. https://doi.org/10.1016/j.petrol.2005.06.007.

Cai, C., Hu, G., Li, H., et al., 2015. Origins and fates of H_2S in the Cambrian and Ordovician in Tazhong area: Evidence from sulfur isotopes, fluid inclusions and production data. Mar. Petrol. Geol. 67, 408–418. https://doi.org/10.1016/j.marpetgeo.2015.05.007.

Cai, C., Hu, W., Worden, R.H., 2001. Thermochemical sulphate reduction in Cambro-Ordovician carbonates in Central Tarim. Mar. Petrol. Geol. 18 (6), 729–741. https://doi.org/10.1016/S0264-8172(01)00028-9.

Cai, C., Li, H., Li, K., et al., 2022. Thermochemical sulfate reduction in sedimentary basins and beyond: A review. Chem. Geol. 607, 121018. https://doi.org/10.1016/j.chemgeo.2022.121018.

Cai, C., Wang, D., 2024. Thermochemical sulfate reduction by ethane in the Ordovician from the Daniudi gasfield results in Hg isotope fractionation. Natural Gas Geoscience Meeting, Ruian, Zhejiang.

Cai, C., Worden, R.H., Bottrell, S.H., et al., 2003. Thermochemical sulphate reduction and the generation of hydrogen sulphide and thiols (mercaptans) in Triassic carbonate reservoirs from the Sichuan Basin, China. Chem. Geol. 202, 39–57. https://doi.org/10.1016/S0009-2541(03)00209-2.

Cai, C., Xie, Z., Worden, R.H., et al., 2004. Methane-dominated thermochemical sulphate reduction in the Triassic Feixianguan Formation East Sichuan Basin, China: Towards prediction of fatal H_2S concentrations. Mar. Petrol. Geol. 21 (10), 1265–1279. https://doi.org/10.1016/j.marpetgeo.2004.09.003.

Cai, C., Zhang, C., Cai, L., et al., 2009. Origins of Palaeozoic oils in the Tarim Basin: Evidence from sulfur isotopes and biomarkers. Chem. Geol. 268 (3–4), 197–210. https://doi.org/10.1016/j.chemgeo.2009.08.012.

Cai, C., Zhang, C., He, H., et al., 2013. Carbon isotope fractionation during methane-dominated TSR in East Sichuan Basin gasfields, China: A review. Mar. Petrol. Geol. 48, 100–110. https://doi.org/10.1016/j.marpetgeo.2013.08.006.

Dai, J., 1993. Characteristics of carbon and hydrogen isotopes in natural gas and identification of various natural gas types. Nat. Gas Geosci. 1–40. https://doi.org/10.11764/j.issn.1672-1926.1993.02.1 (in Chinese).

Dai, J., 1985. Distribution, classification and origin of natural gas with hydrogen sulphide in China. Acta Sedimentol. Sin. 3 (4), 109–120 https://doi.org/CNKI:SUN:CJXB.0.1985-04-009 (in Chinese).

Dai, J., Li, J., Luo, X., et al., 2005. Stable carbon isotope compositions and source rock geochemistry of the giant gas accumulations in the Ordos Basin, China. Org. Geochem. 36, 1617–1635. https://doi.org/10.1016/j.orggeochem.2005.08.017.

Dai, J., Ni, Y., Hu, G., et al., 2014. Stable carbon and hydrogen isotopes of gases from the large tight gas fields in China. Sci. China Earth Sci. 57, 88–103 (in Chinese).

Dou, L., Li, Z., Guo, C., et al., 2024. Resource distribution, geological characteristics, and exploration and development progress of global high-sulfur gas reservoirs. Nat. Gas. Ind. 2024 44 (11), 11–23 https://doi.org/10.3787/j.issn.1000-0976.2024.11.002 (in Chinese).

Fei, A., Zhu, G., Zhang, S., et al., 2010. Global distribution hydrogen sulphide-bearing natural gas and the major factors controlling its formation. Earth Sci. Front. 17 (1), 350–360.

Goldhaber, M.B., Orr, W.L., 1995. Kinetic controls on thermochemical sulfate reduction as a source of sedimentary H_2S. In: Vairavamurthy, M.A., Schoonen, M.A.A. (Eds.), Geochemical Transformations of Sedimentary Sulfur. American Chemical Society Symposium Series, vol 612. American Chemical Society, Washington D. C., pp. 412–425

Goldstein, R.H., 2001. Fluid inclusions in sedimentary and diagenetic systems. Lithos 55, 159–193. https://doi.org/10.1016/S0024-4937(00)00044-X.

Guo, H., Liu, M., Wang, Y., et al., 2022a. The effect of thermochemical sulfate reduction of n-pentane and condensate on the chemical and isotopic compositions of gases: implications for the organic reactant and reaction extent. Mar. Petrol. Geol. 145, 105916. https://doi.org/10.1016/j.marpetgeo.2022.105916.

Guo, H., Liu, M., Wang, Y., et al., 2022b. Characterization of chemical and carbon isotopic compositions of gases during thermochemical sulfate reduction and implications for gas origin and content. Sci. Rep. 12, 9118. https://doi.org/10.1038/s41598-022-13017-3.

Hao, F., Guo, T., Zhu, Y., et al., 2008. Evidence for multiple stages of oil cracking and thermochemical sulfate reduction in the Puguang gas field, Sichuan Basin, China. AAPG Bull. 92 (5), 611–637. https://doi.org/10.1306/01210807090.

He, H., Guo, X., Zhao, Z., et al., 2022. New understandings on gas accumulation and major exploration breakthroughs in subsalt Ma 4 member of Ordovician Majiagou Formation, Ordos Basin, NW China. Petrol. Explor. Dev. 49 (3), 429–439. https://doi.org/10.11698/PED.20210659.

Heydari, E., 1997. The role of burial diagenesis in hydrocarbon destruction and H_2S accumulation, Upper Jurassic Samckover Formation, black creek field, Mississippi. AAPG (Am. Assoc. Pet. Geol.) Bull. 81 (1), 26–45. https://doi.org/10.1306/522B427B-1727-11D7-8645000102C1865D.

Heydari, E., Moore, C.H., 1989. Burial diagenesis and thermochemical sulfate reduction, Smackover Formation, Southeastern Mississippi Salt Basin. Geology 17 (12), 1080–1084. https://doi.org/10.1130/0091-7613(1989)0172.3.CO;2.

Hu, A., Shen, A., Zhang, J., et al., 2022. Source-reservoir characteristics of high-frequency cyclic carbonate–evaporite assemblages: A case study of the lower and middle assemblages in the Ordovician Majiagou Formation, Ordos Basin. Oil Gas Geol. 43 (4), 943–956. https://doi.org/10.11743/ogg20220416 (in Chinese).

Hu, G., Li, J., Shan, X., et al., 2010. The origin of natural gas and the hydrocarbon charging history of the Yulin gas field in the Ordos Basin, China. Int. J. Coal Geol. 81 (4), 381–391. https://doi.org/10.1016/j.coal.2009.07.016.

Huang, L., Liu, C., Wang, Z., et al., 2025a. An alternative formation mechanism for strike-slip fault in stable intracratonic basin. J. Struct. Geol. 191, 105292. https://doi.org/10.1016/j.jsg.2024.105292.

Huang, L., Liu, C., Wang, Z., et al., 2025b. Abrupt structural deformation changes from the boundary to the interior of a craton basin: implications for the long-term stability of cratonic blocks. Geol. Soc. Am. Bull. 137 (1–2), 825–840. https://doi.org/10.1130/B37503.1.

Jiang, L., Worden, R.H., Yang, C., 2018. Thermochemical sulphate reduction can improve carbonate petroleum reservoir quality. Geochem. Cosmochim. Acta 223, 127–140. https://doi.org/10.1016/j.gca.2017.11.032.

King, H.E., Walters, C.C., Horn, W.C., et al., 2014. Sulfur isotope analysis of bitumen and pyrite associated with thermal sulfate reduction in reservoir carbonates at the big Piney-La barge production complex. Geochem. Cosmochim. Acta 134, 210–220. https://doi.org/10.1016/j.gca.2013.11.005.

Kiyosu, Y., Krouse, H.R., 1989. Carbon isotope effect during abiogenic oxidation of methane. Earth Planet Sci. Lett. 95 (3), 302–306. https://doi.org/10.1016/0012-821X(89)90105-2.

Kong, Q., Yao, J., Ren, J., et al., 2024. Sources and exploration potential of Ordovician subsalt natural gas in Ordos Basin. Nat. Gas Geosci. 35 (7), 1187–1201 https://doi.org/10.11764/j.issn.1672-1926.2023.12.009. (in Chinese).

Kong, Q., Zhang, W., Li, J., et al., 2019. Geochemical characteristics and genesis of Ordovician natural gas under gypsolyte in Ordos Basin. Nat. Gas Geosci. 30 (3), 423–432. https://doi.org/10.11764/j.issn.1672-1926.2018.12.020 (in Chinese).

Krouse, H.R., Viau, C.A., Eliuk, L.S., et al., 1988. Chemical and isotopic evidence of thermochemical sulfate reduction by light hydrocarbon gases in deep carbonate reservoirs. Nature 333 (6172), 415–419. https://doi.org/10.1038/333415a0.

Li, J., Li, J., Li, Z., et al., 2014. The hydrogen isotopic characteristics of the Upper Paleozoic natural gas in Ordos Basin. Org. Geochem. 74, 66–75. https://doi.org/10.1016/j.orggeochem.2014.01.020.

Li, J., Li, Z., Zhang, C., et al., 2018. Characteristics and genetic types of the Lower Paleozoic natural gas, Ordos Basin. Mar. Petrol. Geol. 89, 106–119. https://doi.org/10.1016/j.marpetgeo.2017.06.046.

Li, K., George, S.C., Cai, C., et al., 2019. Fluid inclusion and stable isotopic studies of thermochemical sulfate reduction, Upper Permian and Lower Triassic gas-fields, Northeast Sichuan Basin, China. Geochem. Cosmochim. Acta 246, 86–108. https://doi.org/10.1016/j.gca.2018.11.032.

Li, Y., Liu, W., Wang, X., et al., 2021. Potential causes of depleted $\delta^{13}C_{carb}$ excursions in Ordovician marine carbonates, Ordos Basin, China. Mar. Petrol. Geol. 134, 105331. https://doi.org/10.1016/j.marpetgeo.2021.105331.

Liu, D., Feng, Z., Liu, Y., et al., 2016. Geochemistry of the self-generated and self-accumulated gas of Lower Paleozoic in Ordos Basin, China. Nat. Gas Geosci. 27 (10), 1892–1903. https://doi.org/10.11764/j.issn.1672-1926.2016.10.1892 (in Chinese).

Liu, Q., Chen, M., Liu, W., et al., 2009. Origin of natural gas from the Ordovician paleo-weathering crust and gas-filling model in Jingbian gas field, Ordos Basin, China. J. Asian Earth Sci. 35, 74–88. https://doi.org/10.1016/j.jseaes.2009.01.005.

Liu, Q., Jin, Z., Wu, X., et al., 2014a. Origin and carbon isotope fractionation of CO_2 in marine sour gas reservoirs in the eastern Sichuan Basin. Org. Geochem. 74, 22–32. https://doi.org/10.1016/j.orggeochem.2014.01.012.

Liu, Q., Liu, W., Xu, Y., et al., 2007. Geochemistry of natural gas and crude computation of gas-generated contribution for various source rocks in sulige gas field, Ordos Basin. Nat. Gas Geosci. 18 (5), 697–702 https://doi.org/JournalArticle/5aeaba2ec095d70944f0e558 (in Chinese).

Liu, Q., Peng, W., Meng, Q., et al., 2020. Fractionation of carbon and hydrogen isotopes of TSR-altered gas products under closed system pyrolysis. Sci. Rep. 10, 12921. https://doi.org/10.1038/s41598-020-69580-0.

Liu, Q., Worden, R.H., Jin, Z., et al., 2013. TSR versus non-TSR processes and their impact on gas geochemistry and carbon stable isotopes in Carboniferous, Permian and Lower Triassic marine carbonate gas reservoirs in the Eastern Sichuan Basin, China. Geochem. Cosmochim. Acta 100, 96–115. https://doi.org/10.1016/j.gca.2012.09.039.

Liu, Q., Worden, R.H., Jin, Z., et al., 2014b. Thermochemical sulphate reduction (TSR) versus maturation and their effects on hydrogen stable isotopes of very dry alkane gases. Geochem. Cosmochim. Acta 137, 208–220. https://doi.org/10.1016/j.gca.2014.03.013.

Liu, Q., Wu, X., Wang, X., et al., 2019. Carbon and hydrogen isotopes of methane, ethane, and propane: A review of genetic identification of natural gas. Earth Sci. Rev. 190, 247–272. https://doi.org/10.1016/j.earscirev.2018.11.017.

Liu, Q., Zhu, D., Meng, Q., et al., 2018. The scientific connotation of oil and gas formations under deep fluids and organic-inorganic interaction. Sci. China Earth Sci. 61 (3), 507–528. https://doi.org/10.1007/s11430-018-9281-2.

Liu, W., Zhang, D., Wang, X., 2006. Influence of hydrogenation and TSR (thermochemical sulfade reduction) to natural gas isotopic composition. Acta Petrol. Sin. 22 (8), 2237–2242. https://doi.org/10.3969/j.issn.1000-0569.2006.08.014 (in Chinese).

Machel, H.G., 1998. Gas souring by thermochemical sulfate reduction at 140°C: Discussion. AAPG (Am. Assoc. Pet. Geol.) Bull. 82 (10), 1870–1873. https://doi.org/10.1306/1D9BD173-172D-11D7-8645000102C1865D.

Machel, H.G., Krouse, H.R., Sassen, R., 1995. Products and distinguishing criteria of bacterial and thermochemical sulfate reduction. Appl. Geochem. 10, 373–389. https://doi.org/10.1016/0883-2927(95)00008-8.

Munz, I.A., 2001. Petroleum inclusions in sedimentary basins: systematics, analytical methods and applications. Lithos 55, 195–212. https://doi.org/10.1016/S0024-4937(00)00045-1.

Niu, X., Wu, D., Liu, X., et al., 2024. Paleogeographic evolution of the middle and lower assemblages of the Majiagou Formation in the Ordos Basin and the pattern of reservoir distribution. Chin. J. Geol. 59 (3), 625–636. https://doi.org/10.12017/dzkx.2024.044.

Orr, W.L., 1977. Geologic and Geochemical Controls on the Distribution of Hydrogen Sulfide in Natural Gas. Pergramon Press, Oxford, pp. 571–597.

Orr, W.L., 1990. Rate and Mechanism of Non-microbial Sulfate Reduction: Thermochemical Sulfate Reduction. Lecture Note of GRI Workshop.

Prinzhofer, A.A., Huc, A.Y., 1995. Genetic and post-genetic molecular and isotopic fractionations in natural gases. Chem. Geol. 126, 281–290. https://doi.org/10.1016/0009-2541(95)00123-9.

Ren, Z., Qi, K., Li, J., et al., 2021. Thermodynamic evolution and hydrocarbon accumulation in the Ordos Basin. Oil Gas Geol. 42 (5), 1030–1042. https://doi.org/10.11743/ogg20210502 (in Chinese).

Rickard, D., 1997. Kinetics of pyrite formation by the H_2S oxidation of iron (II) monosulfide in aqueous solutions between 25 and 125 °C: The rate equation. Geochem. Cosmochim. Acta 61 (1), 115–134. https://doi.org/10.1016/S0016-7037(96)00321-3.

Seewald, J.S., 2003. Organic-inorganic interactions in petroleum-producing sedimentary basins. Nature 426 (6964), 327–333. https://doi.org/10.1038/nature02132.

Tian, J., Hao, F., Zhou, X., et al., 2014. Charging of the Penglai 9-1 oil field, Bohai Bay Basin, China: Functions of the delta on accumulating petroleum. Mar. Petrol. Geol. 57, 603–618. https://doi.org/10.1016/j.marpetgeo.2014.07.007.

Toland, W.G., 1960. Oxidation of organic compounds with aqueous sulfate. J. Am. Chem. Soc. 82, 1911–1916. https://doi.org/10.1021/ja01493a020.

Wang, Q., Zou, H., Hao, F., et al., 2016. Petroleum charge and entrapment along active faults: study of the accumulation mechanism of the Qinhuangdao 29 oil field on the slope of the Shijiutuo uplift, Bohai Sea. AAPG (Am. Assoc. Pet. Geol.) Bull. 100 (10), 1541–1560. https://doi.org/10.1306/04201615088.

Wang, X., Liu, W., Shi, B., et al., 2015. Hydrogen isotope characteristics of thermo genic methane in Chinese sedimentary basins. Org. Geochem. 83–84, 178–189. https://doi.org/10.1016/j.orggeochem.2015.03.010.

Worden, R.H., Smalley, P.C., 1996. H_2S-producing reactions in deep carbonate gas reservoirs: Khuff Formation, Abu Dhabi. Chem. Geol. 133 (1–4), 157–171. https://doi.org/10.1016/S0009-2541(96)00074-5.

Worden, R.H., Smalley, P.C., Oxtoby, N.H., 1995. Gas souring by thermochemical sulfate reduction at 140 °C. AAPG (Am. Assoc. Pet. Geol.) Bull. 79 (6), 854–863. https://doi.org/10.1306/8D2B1BCE-171E-11D7-8645000102C1865D.

Wu, X., Ding, Z., Yu, Z., et al., 2017. Natural gas reservoir forming conditions and exploration potential of the middle and lower assemblages of the Ordovician Majiagou Formation in the Ordos Basin. In: Proceedings of the National Annual Conference on Natural Gas. Hangzhou, Zhejiang.

Wu, X., Xu, W., Li, R., et al., 2022. Genesis of hydrogen sulfide in Ordovician Majiagou Formation, mid-eastern Ordos Basin: Evidence from fluid inclusions. Acta Pet. Sin. 43 (2), 250–261. https://doi.org/10.7623/syxb202202007 (in Chinese).

Yang, H., Liu, X., 2014. Progress of Paleozoic coal-derived gas exploration in Ordos Basin, West China. Petrol. Explor. Dev. 41 (2), 129–137. https://doi.org/10.11698/PED.2014.02.01 (in Chinese).

Yang, H., Zhang, W., Zan, C., et al., 2009. Geochemical characteristics of Ordovician subsalt gas reservoir and their significance for reunderstanding the gas source of Jingbian gasfield, east Ordos Basin. Nat. Gas Geosci. 20 (1), 8–14. https://doi.org/CNKI:SUN:TDKX.0.2009-01-005 (in Chinese).

Yang, J., Pei, X., 1996. Natural Gas Geology in China Volume IV: Ordos Basin. Petroleum Industry Press, Beijing.

Yang, P., Ren, Z., Fu, J., et al., 2024. A tectono-thermal perspective on the petroleum generation, accumulation and preservation in the southern Ordos Basin, North China. Pet. Sci. 21 (3), 1459–1473. https://doi.org/10.1016/j.petsci.2023.12.006.

Yang, S., Gang, W., Cao, J., et al., 2022. Geochemical characteristics, origin and carbon isotope reversal of the presalt natural gas in the Lower Paleozoic Ordovician carbonates, Ordos Basin, China. Mar. Petrol. Geol. 139, 105577. https://doi.org/10.1016/j.marpetgeo.2022.105577.

Yu, C., Huang, S., Gong, D., et al., 2013. Partial reversal cause of carbon and hydrogen isotope compositions of natural gas: A case study in Sulige gas field, Ordos Basin. Acta Pet. Sin. 34 (S1), 91–101. https://doi.org/10.7623/syxb2013S1011 (in Chinese).

Zhang, N., He, D., Sun, Y., et al., 2014. Distribution patterns and controlling factors of giant carbonate rock oil and gas fields worldwide. China Petroleum Exploration 19 (6), 54–65. https://doi.org/10.3969/j.issn.1672-7703.2014.06.007 (in Chinese).

Zhang, T., Amrani, A., Ellis, G.S., et al., 2008. Experimental investigation on thermochemical sulfate reduction by H_2S initiation. Geochem. Cosmochim. Acta 72 (4), 3518–3530. https://doi.org/10.1016/j.gca.2008.04.036.

Zhang, T., Ellis, G.S., Wang, K., et al., 2007. Effect of hydrocarbon type on thermochemical sulfate reduction. Org. Geochem. 38 (6), 897–910. https://doi.org/10.1016/j.orggeochem.2007.02.004.

Zhang, W., Liu, W., Wang, X., et al., 2023. Formation mechanism of heavy hydrocarbon carbon isotope anomalies in natural gas from Ordovician marine carbonate in the Ordos Basin. J. Mar. Sci. Eng. 11, 2176. https://doi.org/10.3390/jmse11112176.

Zhao, W., Liu, W., 2008. Basic Research on the Formation and Distribution of Efficient Natural Gas Reservoirs and the Economic Development of Condensate and Low Efficiency Gas Reservoirs. Science Press, Beijing, pp. 101–102.

Zhou, J., Li, M., Wu, D., et al., 2023. Characteristics and exploration potential of subsalt gas-bearing system in Majiagou Formation of Middle Ordovician in the eastern Ordos Basin. Nat. Gas. Ind. 43 (3), 34–45. https://doi.org/10.3787/j.issn.1000-0976.2023.03.004 (in Chinese).

Zhou, J., Xi, S., Deng, H., et al., 2020. Tectonic-lithofacies paleogeographic characteristics of Cambrian–Ordovician deep marine carbonate rocks in the Ordos Basin. Nat. Gas. Ind. 40 (2), 41–53. https://doi.org/10.3787/j.issn.1000-0976.2020.02.005.

Zhu, G., Fei, A., Zhao, J., et al., 2014. Sulfur isotopic fractionation and mechanism for thermochemical sulfate reduction genetic H_2S. Acta Petrol. Sin. 30 (12), 3772–3786. https://doi.org/CNKI:SUN:YSXB.0.2014-12-025 (in Chinese).